IOPscience iopscience.iop.org

Home Search Collections Journals About Contact us My IOPscience

Polariton and spin dynamics in semiconductor microcavities under non-resonant excitation

This article has been downloaded from IOPscience. Please scroll down to see the full text article.

2007 J. Phys.: Condens. Matter 19 295204

(http://iopscience.iop.org/0953-8984/19/29/295204)

View the table of contents for this issue, or go to the journal homepage for more

Download details:
IP Address: 129.252.86.83
The article was downloaded on 28/05/2010 at 19:49

Please note that terms and conditions apply.

IOP PUBLISHING JOURNAL OF PHYSICS: CONDENSED MATTER

J. Phys.: Condens. Matter **19** (2007) 295204 (30pp) doi:10.1088/0953-8984/19/29/295204

Polariton and spin dynamics in semiconductor microcavities under non-resonant excitation

M D Martín, G Aichmayr[1], A Amo, D Ballarini, Ł Kłopotowski[2] and L Viña[3]

SEMICUAM. Departamento de Física de Materiales, Universidad Autónoma de Madrid, E-28049 Madrid, Spain

E-mail: luis.vina@uam.es

Received 17 April 2007
Published 11 June 2007
Online at stacks.iop.org/JPhysCM/19/295204

Abstract

Semiconductor microcavities offer an ideal scenario to study strong radiation–matter interactions. In this paper we review the temporal dynamics of polaritons in II–VI and III–V based microcavities under non-resonant excitation conditions. We present evidence of final-state stimulated scattering and discuss the spin-dependent emission, which exhibits a remarkably rich behaviour.

(Some figures in this article are in colour only in the electronic version)

1. Introduction

Semiconductor microcavities are very suitable systems to investigate light–matter interaction in confined structures. In a planar microcavity, a quantum well (QW) excitonic state can be brought into resonance with a discrete Fabry–Perot mode of the cavity ($\delta = E_C - E_{QW} = 0$). If their interaction energy is greater than any homogeneous or inhomogeneous broadening of the bare photon or exciton mode, the system is in the strong-coupling (SC) regime, first observed in 1992 by Weisbuch *et al* [1]. In the SC regime, the eigenstates of the system are mixed states of light and matter, called polaritons, and the energy eigenvalues are modified with respect to those of the uncoupled particles. The normal-mode splitting breaks the degeneracy of photons and excitons into lower and upper polariton branches (LPB, UPB). The modification of the spontaneous-emission dynamics of QWs embedded in a planar microcavity, and its detuning dependence, were explained by the strong radiative coupling between the radiant exciton states and the cavity photon modes [2]. The SC regime has attracted great interest because of its importance from a fundamental point of view as well as for possible applications, in particular when the system is excited by non-resonant optical pumping. It was soon realized that bosonic effects, which should be observable in bare quantum wells, could become a reality

[1] Present address: Qimonda Dresden GmbH & Co OHG, Königsbrücker Straße. 180 D-01099, Dresden, Germany.
[2] Present address: Institute of Physics, Polish Academy of Sciences, Aleja Lotnikov 32/46, PL-02668 Warsaw, Poland.
[3] Author to whom any correspondence should be addressed.

 © 2007 IOP Publishing Ltd Printed in the UK

in microcavities. Whereas in the former case the required particle densities to access boson statistics were too high, in the latter systems, however, this is possible due to an altered density of states (DOS) in the strongly coupled polariton system. In recent years, this possibility of achieving a polariton condensation at the bottom of the dispersion relation has elicited great interest [3]. Like excitons, polaritons, due to their integer spin, can be described as bosons, provided that their densities are sufficiently low [4–6]. Whether this approximation is valid or not can be obtained from an inspection of the commutator of the boson operators, which equals approximately $1 - 2\pi a_B^2 n_X$. The deviation of the commutator from unity is directly proportional to the exciton density, n_X, and to the square of the Bohr radius, a_B, i.e. the bosonic approximation is only valid if $2\pi a_B^2 n_X \ll 1$. Kira *et al* [7] calculated the Bose commutator for GaAs QWs that were incorporated into a microcavity and found that it is only close to 1 when $n_X \leqslant 10^{10}$ cm^{-2}. Since the Bohr radius in GaAs QWs is about 150 Å and in CdTe $\sim$ 30 Å, the Bose limit is valid to an exciton density at least one order of magnitude higher in the CdTe system than in the GaAs case. When Bose statistics is valid, one state can be occupied by more than one particle. It can be shown that when the occupation number of such a state reaches 1, the rate at which particles relax from the excited state to the ground state increases exponentially. Therefore this process is called final state stimulation (FSS) of the polariton relaxation. Phonon emission is the most common process invoked in this relaxation, but it was predicted a few years ago [8] that direct polariton–polariton scattering can also lead to FSS.

Experiments on microcavities indeed showed nonlinear emission behaviour in the UPB at positive detunings, $\delta > 0$, which was attributed to FSS [9]. However, this behaviour was reproduced by calculations based on fermionic particles and it was concluded that the observed nonlinear emission was due to lasing of an inverted electron population [7]. These calculations showed that the Bose commutator was well below unity in the density range where the nonlinear effect was observed. Probably, the first work to provide convincing evidence for FSS in microcavities is the seminal paper on the low-temperature photoluminescence (PL) in CdTe-based systems [10]. Later, two experimental works were published almost simultaneously, which indicate FSS relaxation in microcavities at zero and negative detunings [11, 12]: an exponential increase of the gain with increasing excitation density was observed, indicating FSS in III–V microcavities. Further experiments by the British team investigated the angle-resolved and time-integrated emission from the same system [13]. Ciuti *et al* could reproduce the experimental features by calculations made in the polariton basis assuming their bosonic character [14, 15]. In contrast to Huang *et al*, where the dynamics lasted about 100 ps, indicating an incoherent process, Savvidis *et al* observed the gain only during the seeding pulse duration [11], and they verified that the injected and scattered polaritons share the same phase relation between each other, rendering a coherent process, which was identified as parametric scattering of polaritons. A similar result was achieved in four-wave mixing experiments [16] and by continuous wave pumping of the LP also at a certain in-plane wavevector, $\boldsymbol{K}_\parallel$ [17, 18]. Additionally, Stevenson *et al* deduced the occupation number, n_f, directly from measurements and obtained values above 100 for $\boldsymbol{K}_\parallel^{LP} = 0$, estimating the onset of nonlinear emission around $n_f = 1$ [17]. Prior to these experiments, results on non-resonantly excited InGaAs/GaAs microcavities were published, which showed nonlinear emission from the LP at negative detunings [19, 20]. Here the nonlinear increase of emission in the SC regime was observed at densities where the Bose commutator is still close to 1. Thus the assumption that FSS is responsible for the observed effects seems to be justified. Boeuf *et al* reported a nonlinear emission in the SC regime in CdTe microcavities, under non-resonant pulsed excitation [21]. Parametric amplification up to 220 K has also been demonstrated in CdTe-based microcavities and it has been shown that the cut-off temperature of the amplification is determined by the binding energy of the excitons [22]. Evidence for spontaneous formation of a non-equilibrium

Bose condensate of coherent exciton polaritons has been obtained from an analysis of the emission characteristics of CdTe-based microcavities, in the near field and far field, excited by a pulsed and non-resonant optical pump [23]. In this work, it was showed that, above a threshold pumping power, light is emitted by a single quantum state lying at the bottom of the lower exciton–polariton band. The emission intensity increases exponentially with pump power and its linewidth becomes narrower than the cavity mode width. Furthermore, near-field spectroscopy shows that the stimulated emission comes from several bright spots in the cavity plane. A nonlinear increase of the emission intensity into the normal direction, an acceleration of the build-up and decay of the emission, a spatial concentration of the LPs followed by a slow expansion, and an increase in the degree of circular polarization have been interpreted as a signature of a macroscopic polariton condensation. Moreover, a phase transition from a classical thermal mixed state to a quantum-mechanical pure state of exciton polaritons is invoked from the decrease of the second-order coherence function [24, 25].

The case of non-resonant excitation is of particular interest as an intermediate step in the fabrication of potential devices. However, there is a major disadvantage for non-resonant excitation: a bottleneck in the relaxation of polaritons towards $\boldsymbol{K}_{\parallel} = 0$ states. For small polariton populations, the non-resonantly created polaritons accumulate in the bottleneck region, hindering the energy relaxation. However, for large enough populations, strong polariton–polariton interactions trigger the stimulated relaxation to $\boldsymbol{K}_{\parallel} = 0$. This polariton final-state stimulated scattering has proven to be very efficient in overcoming the bottleneck, allowing the observation of very interesting nonlinear effects, such as polariton stimulated emission [18, 26], optical gain [22] and very recently a condensation [23]. In experiments performed in III–V microcavities under cw conditions, it was concluded that nonlinear emission under a single non-resonant excitation is due to collisions and not to stimulated scattering, while under two beams, one out of resonance and the second creating a large occupation factor in the lower polariton final state, the transfer is due to stimulated scattering [27]. However, more recently, in II–VI microcavities, time-resolved photoluminescence measurements under non-resonant excitation have been explained on the basis of stimulated polariton–polariton scatterings towards the lowest-energy polariton states [28]. Last but not least, a massive occupation of the ground state developing from a polariton gas at thermal equilibrium, together with an increase in temporal coherence and a build-up of long-range spatial coherence and linear polarization in CdTe microcavities, has been interpreted as the existence of an spontaneous onset of a macroscopic quantum phase [29]. The Boltzmann dynamics and condensation kinetics of microcavity polaritons, including both polariton–polariton and polariton–phonon scattering, has been fully modelled in a series of recent papers by Haug *et al* [30–32]. The thermodynamics of polariton condensates, including effects of localization, disorder, the internal structure of polaritons and decoherence processes, has been extensively studied by Littlewood and co-workers [33–45].

Recently, the spin properties of polariton systems came under intense investigation since a rich variety of spin-dependent effects has been observed experimentally. The key role played by the use of circularly polarized excitation and detection was demonstrated in the study of the nonlinearities in the emission from the lower polariton branch [19], where, employing resonant excitation into the upper polariton branch, long polariton spin-relaxation times were reported. It was demonstrated that the nonlinearities arise from stimulated scattering into spin-polarized states at the bottom of LPB, the stimulation arising as a result of the bosonic character of the polariton states. The seminal experimental works under both resonant [11, 19, 46, 47] and non-resonant excitation [48–50] stimulated many fruitful discussions about the role of polariton–polariton interactions on the spin dynamics [51–53]. Following the experiments, a wealth of theoretical descriptions of these phenomena has been published [54–58].

In recent years, the study of the linear polarization of the emission has flourished. In II–VI microcavities a dominance of vertically polarized (TE) emission over the horizontally polarized one (TM) for both vertically and horizontally polarized excitation has been described, together with a persistent difference between the two components of the emission leading to a net and constant (within the duration of the emission) linear polarization degree [59]. The angular dependence of the degree of linear polarization of the emission has been studied in InGaAs microcavities: for the LPB emission at negative detunings, an abrupt switch from large positive values of the linear polarization at small angles, close to the growth direction, to large negative values for angles outside a narrow cone of about $\pm 2^\circ$ has been reported and attributed to cavity birefringence effects [60]. An experimentally observed inversion of the linear polarization of the emission with respect to that of the exciting light has been linked to the dominant role of the exchange interaction in the polariton–polariton scattering [61]. The rotation of the plane of polarization of light in a microcavity parametric oscillator has been described by a quantum model, which takes into account polariton–polariton scattering, longitudinal–transverse splitting and self-induced Larmor precession [62]. Very recently, strong experimental evidence of optical anisotropy in a CdTe-based microcavity has been obtained from the pinning of the linear polarization to one of the crystallographic axes independently of the polarization of the excitation. This effect is attributed to a splitting of the polariton doublet at $\boldsymbol{K}_\parallel = 0$, which appears as a consequence of birefringence in the mirrors and/or the cavity [63], in consonance with the anisotropy found in the Rayleigh scattering along different crystallographic axes, which has been attributed to misfit dislocations in the cavity mirrors [64]. Emission experiments performed under elliptical excitation conditions [65] indicate, on one hand, that the polariton spin evolution is characterized by its precession around a self-induced exchange field, which arises from the imbalance between renormalization terms of differently populated single circular polariton states. On the other hand, mutual Coulomb exchange is governed by two kinds of terms. The first ones, acting on polaritons with the same spin, dominate and are responsible for the dynamical repolarization observed in the stimulated scattering regime, as well as for the renormalization of single-polariton states. The second, much smaller, act on polaritons with opposite angular spin and, in a linearly polarized polariton ensemble, they are responsible for the scattering efficiency imbalance toward pairs with polarization parallel or orthogonal to the initial one, leading to strong negative linear polarization of the signal in the stimulated regime. The possibility of switching the linear polarization of a polariton laser by means of an electric field applied along the growth direction of a microcavity has been proposed [66]. Very recently, it has also been shown theoretically that the condensation of spin-degenerated exciton polaritons results in a spontaneous build-up of linear polarization in emission spectra of semiconductor microcavities [67], and therefore that linear polarization is a distinctive feature for polariton condensation under unpolarized pumping. If spin degeneracy is lifted, an elliptically polarized light is emitted by the polariton condensate [68].

Excellent reviews on microcavity polaritons have already been published in the literature: Khitrova *et al* [69] present the nonlinear optical properties of QWs grown inside high-Q Bragg-mirror microcavities, and the experimental observations are explained using a microscopic theory for the Coulomb interacting electron–hole system in the QW that is non-perturbatively coupled to the cavity light field; Savona *et al* [70] make a theoretical analysis of the optical properties of polaritons and emphasize the existence of the two well-defined coupling regimes (strong versus weak); they also analyse in detail the photoluminescence from microcavities considering the polariton formation and realization and the effects of the exciton inhomogeneous broadening; the book by Kavokin and Malpuech [71] covers linear properties of microcavities such as dispersion of polaritons and disorder effects and nonlinear properties,

including parametric amplification, Bose condensation and polariton lasers; two special journal issues [3, 72] cover the latest developments up to the year 2005.

In this paper we review our experiments on the temporal dynamics of polaritons in II–VI and III–V based microcavities under non-resonant excitation conditions. We present evidence of final-state stimulated scattering and discuss the spin-dependent emission, which exhibits a remarkably rich behaviour. The manuscript is organized as follows: section 2 describes the samples and the time-resolved experimental details; section 3 deals with the characterization of the samples; section 4 presents the dynamics of the emission under high-excitation conditions; section 5 discusses the angular dependence of the dynamics of the light emission; section 6 introduces the dynamics of the polarization under circular-polarization conditions, which for the sake of clarity is separated from that under linear polarization; section 7 demonstrates the coexistence of strong- and weak-coupling regimes under circular polarization; section 8 shows a pinning of the linear polarization due to birefringence effects and, finally, the conclusions are presented in section 9.

2. Samples and experiments

We have studied microcavities containing three different types of QWs: (A) $In_{0.06}Ga_{0.94}As$, with GaAs resonators and $GaAs/Al_{0.1}Ga_{0.9}As$ distributed Bragg reflectors (DBRs); (B) GaAs, with $Al_{0.25}Ga_{0.75}As$ resonators and $AlAs/Al_{0.0.35}Ga_{0.65}As$ DBRs; and (C) CdTe, with $Cd_{0.4}Mg_{0.6}Te$ resonators and $Cd_{0.4}Mg_{0.6}Te/Cd_{0.75}Mn_{0.25}Te$ DBRs. Although quantitatively the results depend on the material system, many of the observations are common to the three types of microcavities, and we will present the most relevant results.

Type A microcavities were $3\lambda/2$ wedged microcavities with two sets of three $In_{0.06}Ga_{0.94}As$ QWs, embedded in a GaAs spacer, at the antinodes of the electromagnetic field. The samples were grown by metal-organic vapour-phase epitaxy. Above and below the cavity spacer, $Al_{0.1}Ga_{0.9}As/GaAs$ distributed Bragg reflectors were grown. We will present the results from a sample with a Rabi splitting of 6.6 meV between the upper and lower polariton branches, measured by low-power cw photoluminescence at 5 K.

The type B sample, grown by molecular beam epitaxy, consists of three GaAs QWs embedded in a $3\lambda/2$ $Al_{0.25}Ga_{0.75}As$ Fabry–Perot resonator clad by dielectric mirrors. The top and bottom mirrors are distributed Bragg reflectors made of 20.5 and 24 alternating $AlAs/Al_{0.35}Ga_{0.65}As$ $\lambda/4$ layers, respectively. The exciton-like (X) and cavity-like (C) modes presented a normal-mode-splitting variation between 3.5 and 7 meV.

Results from two different samples of type C will be presented here. Sample C1 is a $\lambda/2$ $Cd_{0.40}Mg_{0.60}Te$ microcavity. Two CdTe QWs of 90 Å are placed in the antinode position of the electromagnetic standing wave. The top/bottom cavity mirrors are DBRs made of 17.5/23 pairs of alternating layers of $Cd_{0.40}Mg_{0.60}Te$ and $Cd_{0.75}Mn_{0.25}Te$. The cavity finesse, extracted from cw reflectivity measurements, amounts to 1200, assuring the excellent quality of the sample. The Rabi splitting is also determined by cw reflectivity measurements and amounts to ∼9.5 meV. Sample C2 is similar to C1, the only differences being the cavity length and the number of QWs, λ and four, respectively, in this case. The Rabi splitting of C2 amounts to ∼14 meV.

In the three cases, a slight variation (introduced by design during growth) of the cavity's thickness along the radial direction of the wafer allowed us to tune the cavity's resonance with the transition in the QWs, and therefore to choose the exciton–cavity energy detuning, δ, by moving the excitation spot across the sample.

Time-resolved photoluminescence experiments were performed with 1.5 ps pulses, provided by a $Ti:Al_2O_3$ laser with a 12 ns repetition time, exciting at an angle $<2°$ with respect

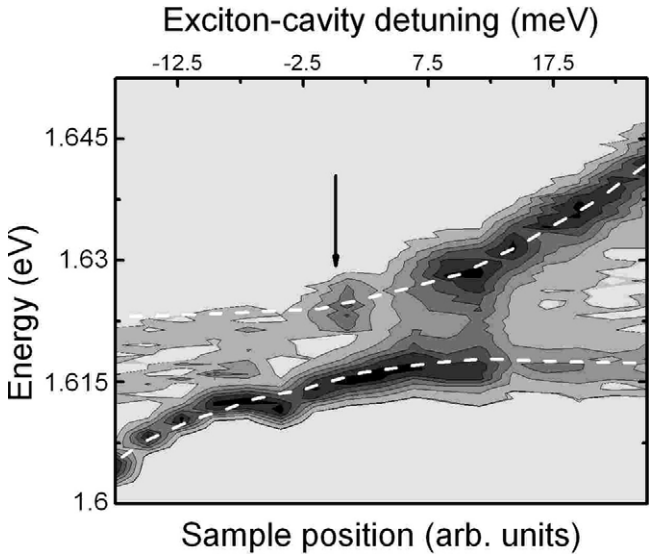

Figure 1. Contour plot of the PL at 10 ps measured in different points of the sample C1. Black = high intensity, light grey = low intensity. The dashed lines correspond to the best fit to equation (1). The arrow indicates the position of the resonance ($\delta = 0$).

to the growth direction. The samples were kept in a cold finger cryostat where T could be changed from 5 to 300 K. For samples B and C1 the PL was collected, for $\boldsymbol{K}_\parallel \leqslant 1 \times 10^4$ cm^{-1}, and time resolved using an up-conversion spectrometer with 2 ps resolution. For samples A and C2 the PL was energy and time resolved using a spectrograph in conjunction with a streak camera, with an overall time resolution below 10 ps. In order to map the PL properties along the polariton dispersion, we measured the emission at different angles θ with respect to the normal of the sample, since $\boldsymbol{K}_\parallel = (E_C/\hbar c)\sin\theta$, where E_C is the energy of a bare cavity photon. The angular resolution was better than 1°, corresponding to wavevector resolution of 10^3 cm^{-1}.

For polarization-resolved measurements, polarization optics ($\lambda/4$ plates, linear polarizers) were used in order to prepare the polarization of the excitation pulse and to analyse the polarization of the emission. The polarization characteristics of the emission are studied through the degree of polarization, $\mathcal{P}$, defined as $\mathcal{P} = \frac{I^{\mathrm{co}} - I^{\mathrm{cross}}}{I^{\mathrm{co}} + I^{\mathrm{cross}}}$, where $I^{\mathrm{co/cross}}$ is the intensity of the polarized components of the emission with polarization parallel/orthogonal to the polarization of excitation (in the case of circular polarization co/cross corresponds to σ^+/σ^-, while for linear polarization the excitation was either vertical (TE) or horizontal (TM)). The degree of polarization is denoted in the following as polarization.

The non-resonant excitation energy is tuned to the first reflectivity dip above the stop band of the DBRs, which varies from sample to sample, to assure equivalent excitation conditions in all the experiments for each sample. The created excitons relax very fast (∼100 fs) by optic phonon emission to polariton states. The scattering processes to thermalize the polaritons close to $\boldsymbol{K}_\parallel \sim 0$ are profusely discussed in [26, 10] and [73], where exciton–exciton Coulomb scattering is shown to play a key role.

3. Sample characterization

The mode splitting between the LPB and UPB at different positions of the samples can be readily obtained from time-resolved PL measurements. Figure 1 shows a contour plot that

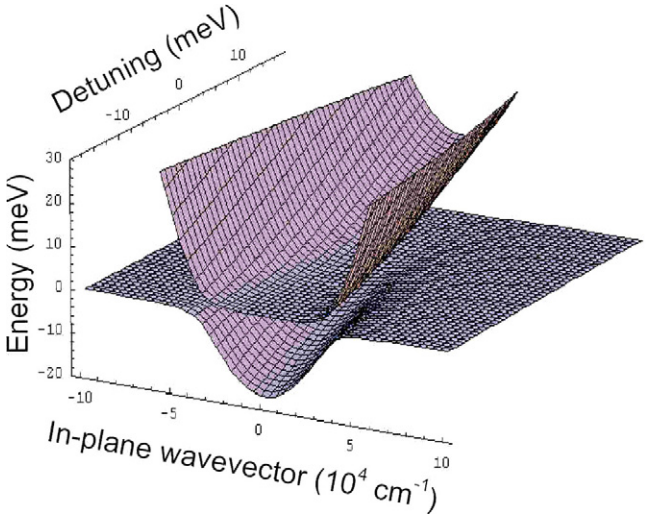

Figure 2. Real part of ω_{LP} and ω_{UP}, from equation (1), as a function of detuning and in-plane wavevector. The exciton energy is assumed as $\omega_{\mathrm{X}} = 0$. The parameters for the calculations are taken from table (1) and $\Omega = 9.5$ meV.

Table 1. Material parameters used for sample C1. Effective masses are given in units of the free electron mass; $a_{2\mathrm{D}}$ is the Bohr radius. The composition-dependent refractive indices are denoted by n (values from [76]).

m_{e}	m_{h}	m_{X}	$a_{2\mathrm{D}}$ (Å)	n_{CdMnTe}	n_{CdMgTe}	n_{QW}	n_{C}
0.096	1.38	1.476	28	2.81	2.5	3.4	2.5

compiles the PL spectra at 10 ps, measured at different points of the sample C1 at $\boldsymbol{K}_{\parallel} = 0$ and 5 K. The PL shows a clearly resolved doublet, which allows determining the energy splitting between the two normal modes and proves the presence of SC of excitons and cavity modes. A clear anticrossing between the bare states is observed, leading to a Rabi splitting of $\Omega \sim 9.5$ meV. The arrow marks the position of resonance ($\delta = 0$), where both polariton branches have equal character of exciton and cavity mode. The region at the left/right of the arrow corresponds to the so-called negative ($\delta < 0$)/positive ($\delta > 0$) detuning, where the LPB has a stronger cavity-/exciton-like character. The two modes correspond to the solution of the equation [74]

$$\omega^{\pm} = \frac{\omega_{\mathrm{X}} + \omega_{\mathrm{C}} - \mathrm{i}(\gamma + \gamma_{\mathrm{C}})}{2} \pm \sqrt{V^2 + \frac{1}{4}(\omega_{\mathrm{X}} - \omega_{\mathrm{C}}) - \mathrm{i}(\gamma + \gamma_{\mathrm{C}})^2} \tag{1}$$

where ω_{X} and ω_{C} are the exciton and cavity frequencies, respectively, γ is the non-radiative exciton broadening, γ_{C} the cavity mode linewidth, V the coupling strength between the exciton and the cavity mode, and the solutions correspond to the UPB (ω^{+}) and the LPB (ω^{-}). The Rabi splitting is given by

$$\Omega = 2\sqrt{V^2 - \tfrac{1}{4}(\gamma_{\mathrm{C}} - \gamma)^2}. \tag{2}$$

Additionally to the position tuning of the cavity energy, the angle of observation can be scanned in order to probe the $\boldsymbol{K}_{\parallel}$-space of the dispersion. Figure 2 shows the UPB and LPB dispersion surfaces (calculated from equation (1) and table 1) as a function of the tunable

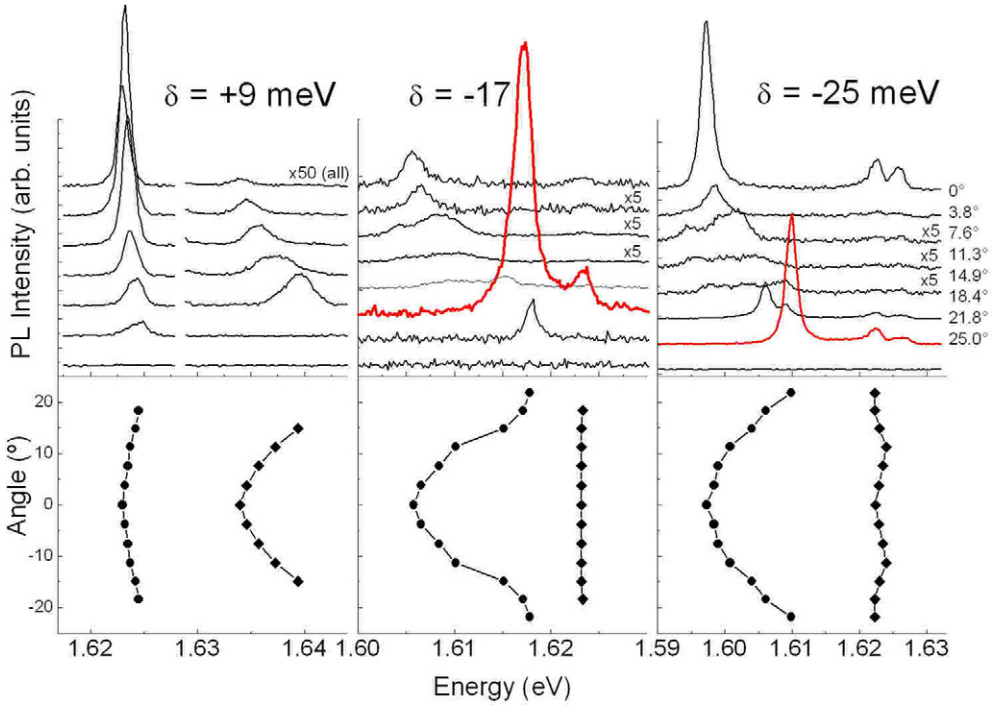

Figure 3. The cw photoluminescence for three different detunings, $\delta = +9, -17$ and -25 meV for sample C1. The lower graphs show the energies of the peaks as a function of detection angle. Values for negative angles are duplicated from those for positive ones and are only drawn for illustration. All spectra were taken at $T = 8$ K and 1 W cm^{-2}. Observation angles were limited to $\sim$22°.

parameters in this system. The range of the parameters roughly corresponds to the detunings and angles that can be addressed by the experimental set-ups used in our experiments. Angle-resolved PL measurements were done by selecting a certain angular portion of the emission with a pinhole, which was placed in front of the collecting lens. An angular resolution of $\sim$1.5° was achieved and the maximum observable angle (limited by the cryostat window) was $\sim \pm 22°$.

Figure 3 shows the PL spectra for three detunings, $\delta = +9, -17$ and -25 meV, as a function of detection angle. At $\delta = -25$ meV, i.e. the bare exciton energy is 25 meV above the cavity, the maximum emission intensity comes from the $\boldsymbol{K}_{\parallel} = 0$ LPB states, and the intensity decays rapidly with increasing angle. However, at 22° the intensity increases again and is only about 20% smaller than the zero-angle value. At $\delta = -17$ meV, the emission at angles higher than zero also decays quickly, but now at 18.4° a pronounced maximum arises which is very sharp in angular distribution, $\Gamma_{\mathrm{FWHM}} \approx 2°$, and is one order of magnitude more intense than the zero-angle emission. These findings demonstrate that a relaxation bottleneck is occurring at these angles. At a positive detuning of $\delta = +9$ meV the angular distribution of the emission of the LPB around $\boldsymbol{K}_{\parallel} = 0$ is very broad (about $\pm 8°$). These results can be compared to the semi-classical model and a very satisfactory agreement is obtained [75]; thus the calculated excitonic and cavity fractions and the LPB density of states DOS can be used to complement the information extracted from the measurements.

It is also clearly observed in figure 3 that the coupling modifies the dispersion relation strongly so that the relaxation from large in-plane wavevector excitons towards $\boldsymbol{K}_{\parallel} = 0$ states

is very slow (bottleneck effect). At negative detunings the in-plane dispersion relation close to $\boldsymbol{K}_{\parallel} = 0$ is extremely steep compared to that of a bare quantum well. Furthermore, the strong coupling produces a distorted S-shape of the LPB band, which is responsible for the large efficiency of pair-polariton scattering, as compared with bare exciton and cavity modes that have quadratic dispersions at small $\boldsymbol{K}_{\parallel}$ hindering pair scattering, because both energy and momentum cannot be conserved simultaneously. The trap in energy close to $\boldsymbol{K}_{\parallel} = 0$ facilitates the existence of FSS polariton–polariton scattering. The effective mass of the polaritons, $\sim 10^{-5} m_{\mathrm{e}}$, several orders of magnitude smaller than the hydrogen atom mass, can allow the condensation of polaritons at temperatures much higher than those required for atom Bose–Einstein condensations. The small density of states at the bottom of the trap also helps to achieve large occupation numbers at densities where the bosonic approximation is still valid and FSS scattering takes place.

The spectral and dynamical properties of the polariton emission can be studied very conveniently by time-resolved PL spectroscopy. Figure 4(a) depicts the low-temperature (5 K) emission spectrum of sample B, for a positive detuning, at low excitation (0.5 W cm^{-2}) obtained 530 ps after the arrival of the excitation pulse (1.706 eV). Two peaks are resolved in the spectrum, which can be satisfactorily fitted with Lorentzian lineshapes, at 1.615 eV ('exciton'-like) and 1.620 eV ('cavity'-like), obtaining a normal mode splitting (NMS) of 5 meV. The characteristic time evolutions of the emission of the LPB ('exciton') and of the UPB ('cavity') are presented in figure 4(b). The initial rise of the PL has several contributions: the first one comes from the binding of the non-resonantly created electron–hole pairs into large $\boldsymbol{K}_{\parallel}$ excitons in the first tens of picoseconds [77]. These excitons scatter into LPB and UPB states and continue reducing their energy and momentum via acoustic-phonon emission. Once they have reached $\boldsymbol{K}_{\parallel} = 0$ states, the PL reaches its maximum value. This $\boldsymbol{K}_{\parallel} = 0$ population exponentially disappears because of radiative recombination and escape of the photons from the cavity. One can see in figure 4(b) that the time dependence is very similar for both polariton branches: the rise and decay times of the PL are slow. The solid lines in the figure are fits with a four-level model, which considers an initial reservoir of large $\boldsymbol{K}_{\parallel}$ exciton–polaritons. The relaxation towards $\boldsymbol{K}_{\parallel} \sim 0$ states is taken into account by the non-radiative decay of the reservoir population to UPB or LPB states. This non-radiative decay is characterized by $\tau_{\mathrm{r}}^{\mathrm{U}}$ and $\tau_{\mathrm{r}}^{\mathrm{L}}$, which are the rise time of the PL emitted by the UPB and the LPB, respectively. This non-radiative decay builds the UPB and LPB populations. The radiative decay from these states is characterized by $\tau_{\mathrm{d}}^{\mathrm{U}}$ and $\tau_{\mathrm{d}}^{\mathrm{L}}$, which are the decay time of the PL emitted by the UPB and the LPB. This simple model allows extracting both the rise and the decay times of the LPB and of the UPB. A detailed study of these characteristic rise and decay times as a function of NMS has revealed almost no dependence on this splitting, in agreement with the results of Abram and co-workers [78] and of Sermage *et al* [2] for the case of positive detunings ($\delta > 0$). The characteristic times extracted from the four-level model fit are summarized in the figure. These times have to be considered just as a first approximation to the polariton dynamics, especially in the case of the rise time, due to the simple relaxation processes considered in the model. More sophisticated models, which take into account the relative exciton–photon composition of the UPB and LPB states, have to be considered to give an accurate description of the recombination dynamics.

4. Emission dynamics under high-excitation conditions

With increasing excitation density, drastic changes are observed in the time-resolved spectra as well as in the recombination dynamics. At low power densities, both the LPB and UPB have a similar dependence on power (slightly larger that linear). In contrast, the dependence

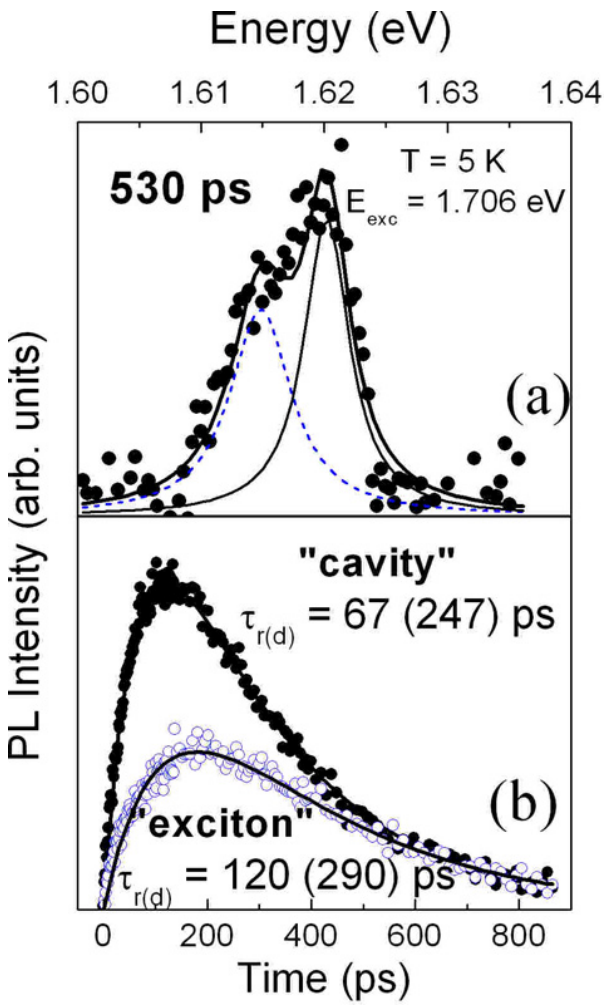

Figure 4. (a) PL spectra measured at 5 K, 530 ps after excitation with pulses of 1.706 eV and a power density of 12 Wcm^{-2}, for sample B at a positive detuning. The lines depict the best fit to Lorentzian lineshapes for the exciton-like (dashed) and cavity-like (solid) components. (b) Time evolution of the cavity-like mode (solid points) and exciton-like mode (open points). The lines depict the best fit with a four-level model. The rise (decay) times of both traces are given indicated as $\tau_{r(d)}$.

of the LPB emission on power shows a threshold. Figures 5(a) and (b) display two PL spectra for sample B, measured 100 ps after excitation, below (○, 7 W cm^{-2}) and at the threshold (●, 20 W cm^{-2}), respectively. At low power, the cavity-like mode (C) is at higher energy that the exciton-like mode (X), i.e. $\delta > 0$, similar to the situation found in cw experiments. Although the LPB is not clearly resolved at 100 ps, the NMS becomes apparent at longer times, when both branches have comparable intensities. At high powers, the situation is reversed and the LPB/UPB has photonic/excitonic character, i.e. $\delta < 0$. The LPB can be clearly resolved for excitation densities $I \geqslant 14$ W cm^{-2} as a very narrow peak at 1.621 eV (marked as C in figure 5(b)), and it sharpens with increasing density, up to a certain threshold I_{th}, reducing its width by a factor of ∼4. This narrowing also occurs for the UPB, but its linewidth is only reduced by a factor for ∼2. The NMS is practically independent of power.

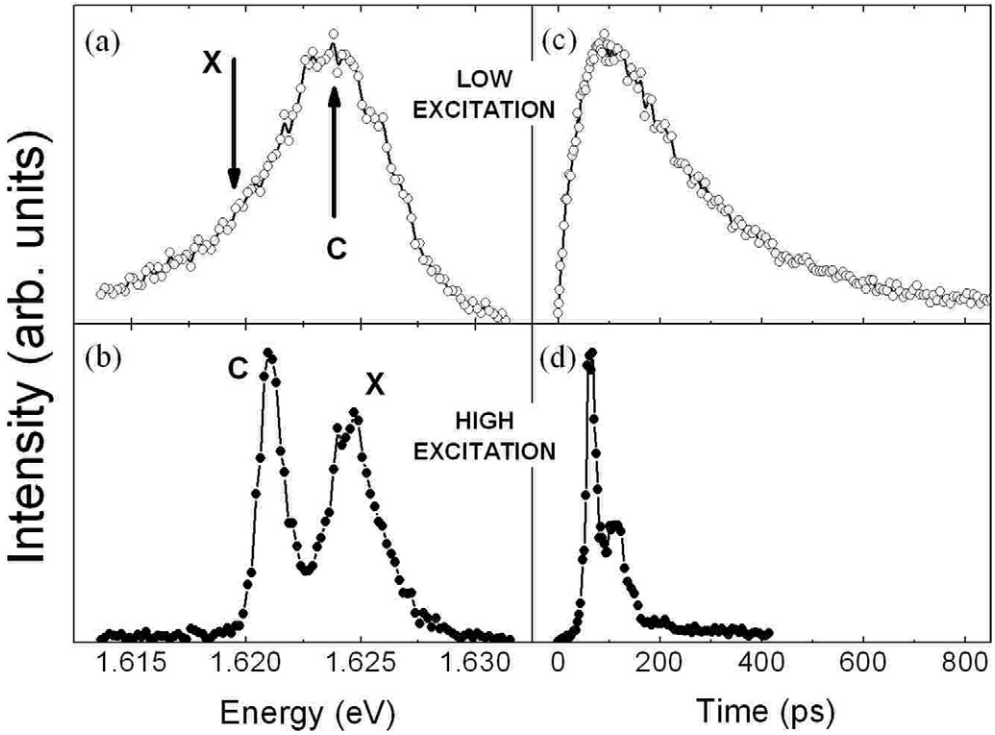

Figure 5. (a) PL spectra measured at 5 K, 100 ps after excitation with a power density of 7 W cm^{-2}, for sample B at a positive detuning. (b) PL spectra measured 100 ps after excitation with a power density of 20 W cm^{-2}. (c) Cavity-mode evolution for an excitation density of 7 W cm^{-2}. (d) Cavity-mode time evolution for an excitation density of 20 W cm^{-2}.

The time evolution is also strongly affected by an increase of excitation density, as shown in figures 5(c) and (d). For small excitation densities (○, 7 W cm^{-2}) the time evolution is similar to that typical of QWs under non-resonant excitation: the emission is characterized by slow rise and decay times [79, 80]. For larger excitation (●, 20 W cm^{-2}), the rise and decay times are faster, and a delay time of ∼30 ps is needed to reach the nonlinear emission regime. This onset in the PL might be related with the bottleneck in the relaxation of polaritons towards $\boldsymbol{K}_{\parallel} = 0$ states [81]. The rapid rise of the PL observed above threshold is interpreted in terms of stimulated scattering, which enhances the build-up of the polariton $\boldsymbol{K}_{\parallel} = 0$ population.

As mentioned above, the LPB and UPB emission energies at short times are higher than those observed at long times, and there is an exchange of the excitonic/photonic character of the two polariton branches with increasing delay time. Figure 6 depicts the emission energies of both polariton branches as a function of time for an I_{th} excitation power. At short times (<100 ps), the UPB has an excitonic character (X) while the LPB has a photonic character (C). As the polariton population decreases at longer times, due to its recombination, the LPB recovers its exciton-like character (X) and the UPB its photon-like character (C), as was determined by cw and long-delay time-resolved experiments performed under low excitation densities. The excitonic part of the polariton is the one that red shifts with time, while the shift of the cavity mode is negligible, as expected from its electromagnetic character. Similar shifts of excitons have been observed in bare QWs and have been attributed to exciton–exciton interaction [82–84]. A clear anticrossing of the UPB and the LPB is observed at

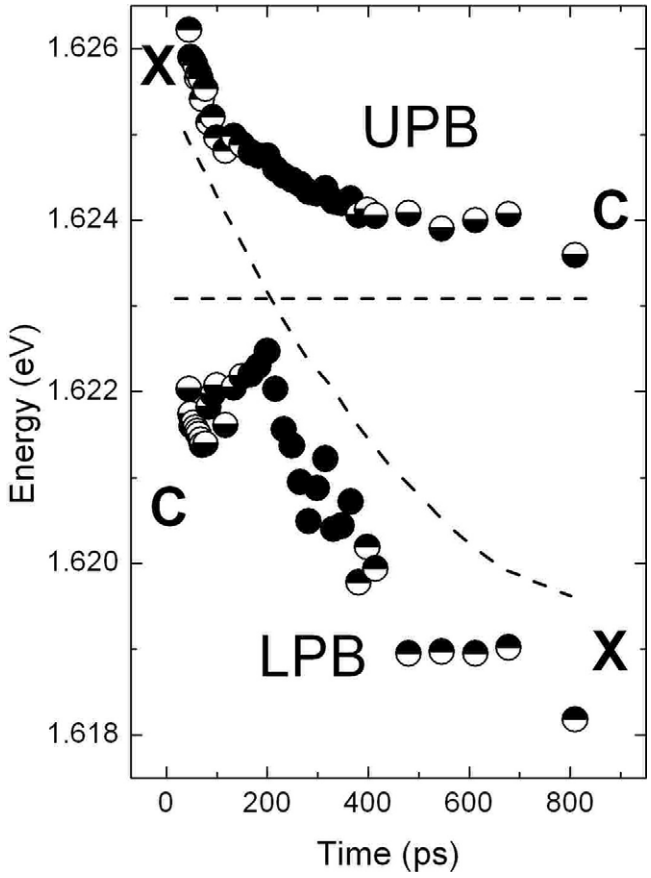

Figure 6. Energy positions of both polariton branches for sample B as a function of time for a power density of 20 W cm^{-2}. An anticrossing is clearly observed at ∼200 ps. The dashed lines are a guide to the eye.

∼200 ps. This dynamical shift of the exciton obtains negative detunings at short times, before the anticrossing takes place. The blue shift, observed at short times in our experiments, is a manifestation of many-body effects and therefore one could expect that at high exciton densities the exciton–cavity coupling would be strongly reduced. The subject of nonlinear emission in III–V semiconductor microcavities has been controversial regarding the existence of polaritons under non-resonant excitation, due to bleaching at high densities [11, 19, 20, 69, 85]. However, the observation of an anticrossing in time indicates that, in this sample with GaAs QWs, the decrease of the exciton oscillator strength with increasing exciton population is not enough to destroy the exciton–cavity strong coupling and is a signature of the persistence of the polaritons.

The four effects just mentioned, linewidth reduction, excitation density threshold, acceleration of the dynamics and, especially, the anticrossing in time, suggest that the PL observed above I_{th} can be attributed to polariton stimulated emission. In addition, the curvature (second derivative with respect to the delay time) of the very initial rise of the LPB time evolution shows important changes with increasing excitation power. It has been shown that in sample B [49], the sign of the curvature changes from negative to positive around the excitation density threshold for the nonlinear processes mentioned above. A further increase of the excitation density leads to a progressive increase of the curvature. The curvature shows

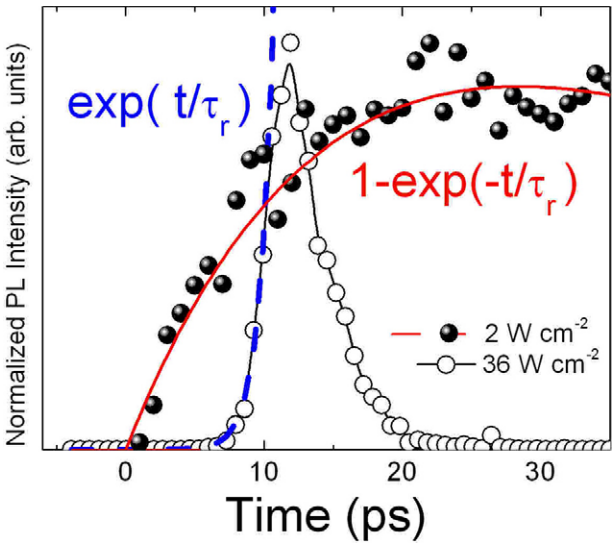

Figure 7. Initial time evolution of the photoluminescence for sample C1 at two different excitation densities: 2 W cm^{-2} (hollow symbols) and 36 W cm^{-2} (full symbols) at $T = 5$ K and $\delta = -13.2$ meV. The lines represent a fit of the initial rise to the functions shown in the figure.

a small dependence on NMS: its absolute value, for a given excitation density, increases with decreasing splitting. This fact is linked with the reduction of the excitation density threshold with decreasing positive detuning. A similar effect is also observed in CdTe-based microcavities: figure 7 depicts the initial rise of the emission of sample C1 for $I_{\mathrm{exc}} = 2$ W cm^{-2} (hollow symbols) and 36 W cm^{-2} (full symbols) at a negative detuning of $\delta = -13.2$ meV. Under low excitation density, the rise of the PL is similar to the one of a bare QW, and it follows a standard three-level model where the rise is proportional to $N_{\mathrm{exc}}(1 - \exp(-t/\tau_{\mathrm{r}}))$ and the curvature is clearly negative. However, when $I_{\mathrm{exc}} = 36$ W cm^{-2}, the curvature becomes positive and the rise can be fitted by a function $\exp(t/\tau_{\mathrm{r}})$. Stimulated relaxation to the ground state ($\boldsymbol{K}_{\parallel} = 0$) leads to an exponentially increasing ground-state population, which accordingly leads to an exponentially increasing emission. Thus our data strongly indicate that FSS is indeed the underlying process of the observed dynamics. Another criterion to prove this assumption is the dependence of the intensity of the emitted light on excitation density, which also shows an exponential increase with excitation power [52, 75]. A similar exponential growth has been reported and interpreted in terms of FSS scattering [11], as is characteristic of a bosonic system when the occupancy of the final state approaches unity. Also in the CdTe system, the linewidth (full width at half maximum extracted from a Gaussian fit of the energy spectrum) of the LP emission shows a strong reduction with increasing power, which in our case is limited by the spectral resolution of the experimental setup. Recently, a reduction of approximately two orders of magnitude in the polariton emission linewidth with the excitation power has been theoretically predicted and interpreted as a characteristic feature of polariton lasing [86].

5. Angular dependence of the dynamics of the light emission

Up to now, we have been discussing the emission of the light at $\boldsymbol{K}_{\parallel} = 0$ for various types of microcavities. Let us focus now in this section on the behaviour of the light emission

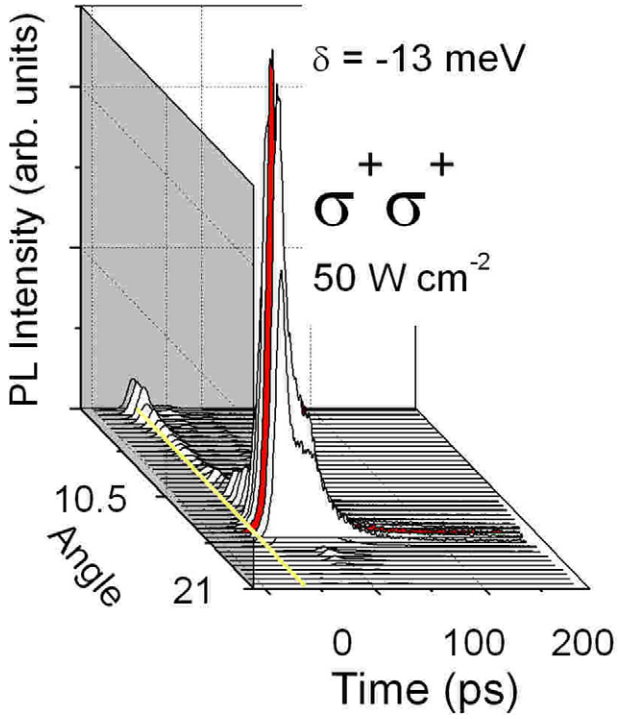

Figure 8. Time evolution of the PL from the LPB of sample C2 as a function of detection angle for co-polarized excitation/detection, an excitation density of 50 W cm^{-2}, and a detuning of $\delta = -13$ meV. The trace of the maximum intensity is shadowed. The line in the horizontal plane indicates zero time.

along the LPB dispersion. Figure 8 depicts the time evolution of the σ^+-polarized emission for sample C2 at a negative detuning of -13 meV, in the nonlinear regime (excitation density 50 W cm^{-2}), under σ^+-polarized, non-resonant excitation. The non-resonant excitation of the sample creates excitons that rapidly relax into polaritons in the cavity. The emission starts at $\boldsymbol{K} \sim 0(0°)$: at early times the dynamics of the light emission is governed by FSS scattering, which is responsible for the very fast rise and decay times of the PL. The bosonic character of the mechanism governing the relaxation is evidenced by an exponential increase of the PL intensity from the photon-like LPB with excitation power, similar to that observed in pump-and-probe [11] and cw PL experiments [17] and attributed to FSS. However, this behaviour is transient, and at later times the maximum intensity of the emission occurs at an angle of 15.4° ($\boldsymbol{K}_\parallel \sim 2 \times 10^4$ cm^{-1}, shadowed trace), giving rise to a ring emission, which has also been observed in resonant excitation cw [73, 87] and time-resolved experiments [88]. In our case, the pulsed excitation at moderately high powers creates a large population and, therefore, the emission starts at $\boldsymbol{K}_\parallel = 0$, assisted by FSS. The resulting decrease of population, through the very fast emission dynamics, shifts the emission to larger $\boldsymbol{K}_\parallel$ values, in agreement with the theoretical predictions [73].

More striking is the observation of strong oscillations in the emission intensity shown in figure 9. The period of the oscillation is ∼30 ps, and it is independent of the observation angle and helicity of the emitted light. The trace corresponding to an angle of 6° reveals that the intensity of the emission collapses and revives, a behaviour never reported before, to the best of our knowledge, in any time-resolved emission of a semiconductor heterostructure, but

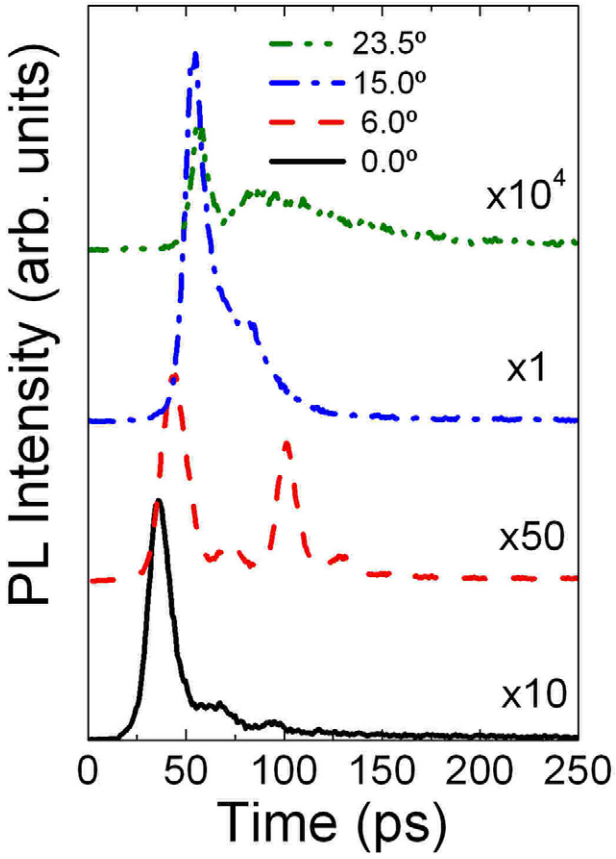

Figure 9. Time evolution traces of the PL from the LPB at $K_{\parallel} = 0$ of the C2 microcavity at a detuning of −13 meV for different angles. The traces are enlarged by the factor shown in the figure. Note the oscillatory behaviour with a period of ∼30 ps.

reported in an atomic Bose–Einstein condensate [89]. At 15°, where the maximum intensity as a function of $K_{\parallel}$ is obtained, a beating is also observed. When the angle of observation is further increased and the excitonic reservoir is approached, the intensity of emission decreases drastically, and after the first beat a slow decaying behaviour is obtained, typical of excitonic emission. The energy scale corresponding to the beat period is 136 μeV, which does not compare to any characteristic energy of our microcavity. A similar beat period, reported recently for wire-shaped microcavities [90], has been attributed to uniaxial strain in the QW plane resulting from the cavity patterning to form wires. However, this cannot be the origin of the oscillations in our planar structures. Remarkably, these oscillations are *in phase*, so they cannot be caused by any kind of beats between σ^+ and σ^--polarized polariton states. The intensities of σ^+- and σ^--components of the PL signal are rather similar, indicating that spin-relaxation of polaritons was quite efficient and that their ± 1 spin states are nearly equally populated. However, the population of these two 'bright' states oscillates with a period of about 30 ps. These oscillations survive over 100 ps, which exceeds by two orders of magnitude the radiative life-time of exciton–polaritons in the photon-like part of their lower dispersion branch. On the other hand, the oscillations closely resemble the beats between bright- and dark-exciton states observed by Renucci *et al* [91]. But in contrast with the Renucci experiment, no

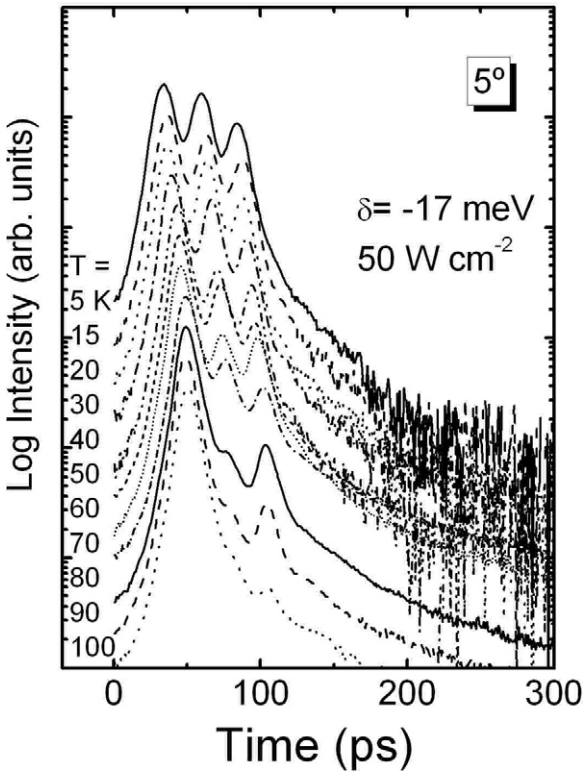

Figure 10. Temporal evolution, on a semi-logarithmic scale, of the photoluminescence at an angle of 5° for sample C2 at a detuning of −17 meV, under non-resonant pumping at high excitation, for different temperatures.

magnetic field has been applied to the sample in our case. Also, the effect we have observed is strongly nonlinear: at low pumping intensities we do not observe any beats; they only appear at strong enough pumping. These experimental facts make us conclude that in the nonlinear regime some new mixing mechanism appears that allows for the dark states to be populated and leads to quantum beats between dark excitons and exciton–polaritons. This mechanism must conserve the spin and optical coherence in the system; otherwise quantum interference between different states would be impossible. Recently, these results have been interpreted as arising from nonlinear coupling of optically active and dark crystal states [92]. One should mention that the oscillations are observed, for the same detuning, at different positions in the sample, which rules out local structure in the polariton spectrum due to polariton localization or the existence of weakly radiative localized excitons as their origin. Recently, these oscillations have also been observed under resonant excitation at the UPB [93].

In order to demonstrate the robustness of the coherent interaction leading to the quantum beats between dark excitons and exciton–polaritons, we present in figure 10 the temperature dependence of the PL time-traces for a detuning of −17 meV and an emission angle of 5° in the nonlinear regime. Different traces, which have been displaced vertically for clarity, for temperatures ranging from 5 to 100 K are plotted in a semi-logarithmic scale. The beats are clearly observed up to the highest temperature shown in the figure, indicating that the coherence is maintained in spite of the increased phonon population. The increase of temperature increases the beating time slightly (15% from 5 to 100 K). The beats between

exciton–polaritons and spin-forbidden ('dark') exciton states take place in a nonlinear regime due to polariton–polariton and exciton–exciton collisions. Remarkably, these collisions conserve the spin and coherence in the system that allows for observation of a new kind of optical parametric oscillations. The long-living coherence in our system is a consequence of the strong bottleneck effect that makes polaritons spend the majority of their lifetime in the exciton-like part of their lower dispersion branch, having a low probability of radiative escape.

6. Polarization dynamics of the emission

The spin dynamics of cavity polaritons in the strong coupling regime has been experimentally studied by means of time- and polarization-resolved spectroscopy in the last decade. Let us discuss here the main effects that are observed in time-resolved PL experiments.

The analysis of the PL emitted after excitation with circularly polarized light is commonly used to study the properties of the third component of the total angular momentum J_Z, which will be called spin in the following [94, 95]. A σ^+ excitation light will mainly populate the $+1$ spin level of the system. After that, a -1 spin population will appear as a result of the spin flip mechanisms, which eventually equalize both spin populations. The recombination of this -1 spin population will result in a σ^--polarized emission. In the case of the spin relaxation of cavity polaritons, their mixed radiation–matter character has to be considered. Since there is no mechanism that changes the spin of its photonic part, the spin relaxation of polaritons occurs through the spin relaxation of their excitonic component.

For excitons in bare QWs, the polarization reaches its maximum value just after excitation and then decays exponentially to zero (see the inset in figure 11) [79, 80]. On the other hand, in microcavities, due to the complex nature of polaritons, one expects the spin dynamics of this mixed state to be different from that of bare excitons or photons. This fact is documented for sample B in figure 11, which depicts the time evolution of the polarization of the cavity mode for two different excitation densities below ($0.33I$th, solid symbols) and above ($2I_{\rm th}$, open symbols) the nonlinear emission threshold. In contrast with the monotonically decreasing behaviour of $\mathcal{P}$ found in bare QWs, a maximum is observed at a finite time after excitation. The polarization at $t = 3$ ps is $\sim$10%, which means that, after the relaxation of polaritons to $\boldsymbol{K}_\parallel = 0$ states, only 55% of the total population is in the $+1$ spin state. Such a small value of $\mathcal{P}$ is mainly due to the non-resonant excitation conditions. $\mathcal{P}_{\rm max}$ is reached in 60–100 ps, and its value increases with excitation density. The fact that a finite time is needed to reach $\mathcal{P}_{\rm max}$ implies that there must be a new scattering mechanism that favours polaritons with $+1$ spin, and thus competes with spin relaxation and tends to prevent equalization of both spin populations. At very low powers, the relaxation of large in-plane wavevector excitons is governed by the emission of acoustic phonons, which has no spin dependence. At high powers, the new mechanism can be interpreted as polariton–polariton scattering, which is stimulated by the polariton final-state population [16]. The increase of $\mathcal{P}_{\rm max}$ with excitation density provides evidence that there is an enhancement of the scattering to the $+1$ spin state. The stimulation does not occur for the σ^--polarized LPB emission, which also shows a time evolution with rise and decay times much longer than those observed in the nonlinear regime for the σ^+ emission.

For excitation densities above the threshold, the time evolution of the cavity-mode polarization displays a much richer behaviour. The LPB polarization reaches values as high as 95% when entering into the nonlinear emission regime. In contrast, for the UPB, although it shows a similar behaviour, its polarization is only 60%. After the initial rise of the polarization, once the maximum is reached, its dynamics is strongly dependent on NMS. For small exciton–cavity detunings (4.5 meV), such as the one shown in figure 11, a negative dip (-60%) is observed at $\sim$150 ps, which is absent for larger NMS [48]. The remarkable change in the

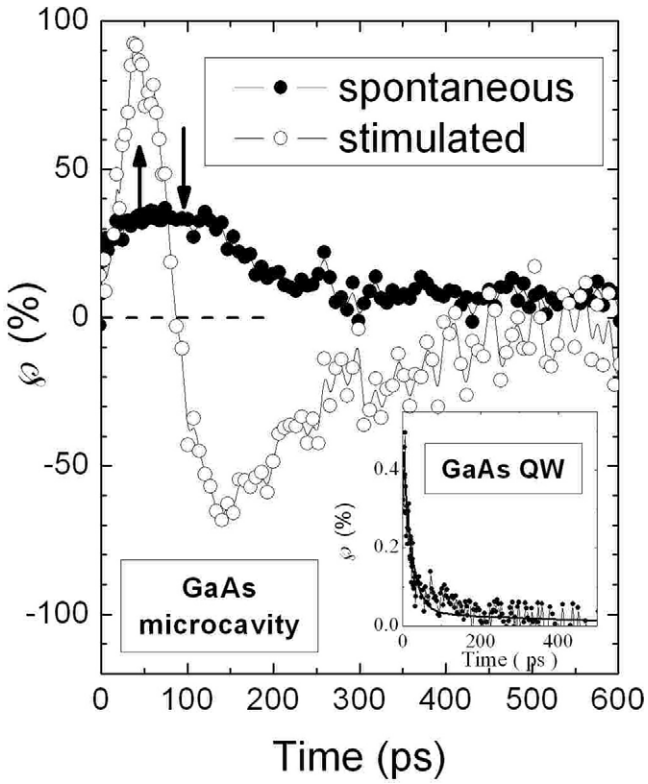

Figure 11. Time evolution of the cavity-mode polarization of sample B for an excitation density of 7 W cm^{-2} (solid points) and 40 W cm^{-2} (open points). The arrows point to the maxima of the polarization. The inset shows a typical time evolution of the polarization in a GaAs quantum well for comparison.

state of polarization of the emitted light from +80% to −60%, taking place in a very short time (∼100 ps), is unique. A similar phenomenon has been reported for QWs [96, 97] and is attributed to an anisotropic spin-splitting of localized excitons, induced by the long-range electron–hole exchange interaction. In our case the splitting could be due to birefringence effects, as discussed in section 8.

Once the minimum of $\mathcal{P}$ is reached, the polarization dynamics becomes slower: by then the polariton population has decreased by a factor 5–10 (depending on the power density) and the remaining +1 spin population is too small to give rise to stimulation. Under these conditions, only the usual spin–flip mechanisms govern the polarization, which decreases steadily. It should be mentioned that excitation with σ^- yields identical results to those of the σ^+ excitation discussed above, as expected from time reversal symmetry arguments. The sign reversal of the polarization is also observed for the σ^- excitation and it is also the majority spin population (−1 in this case) the only one that undergoes stimulation.

Similar effects are also observed in II–VI microcavities. The time evolution of the emission for sample C1 is presented in figure 12 for different detunings, where solid (dashed) lines show the co-(counter-) polarized components. The left panels correspond to the LPB under low excitation conditions: the increase in the decay rate is clearly seen going from positive ($\delta = +15$ meV) to negative ($\delta = -21$ meV) detunings, while the difference in intensity of both polarized components is very small and independent of δ. However, this situation changes

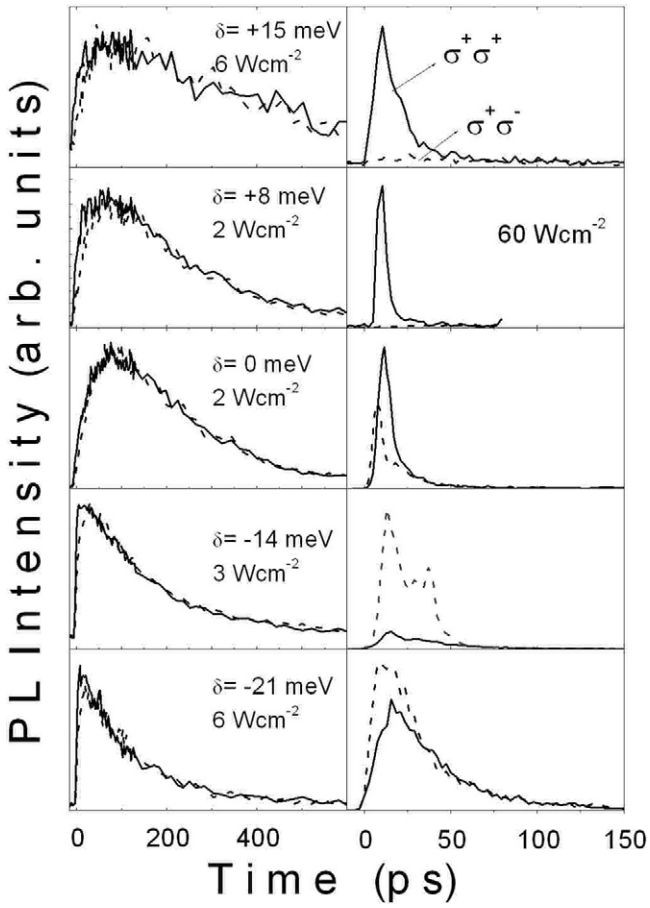

Figure 12. PL emission dynamics for sample C1 at different detunings from $\delta = -21$ to $+15$ meV, for two excitation densities at each detuning. The scale of the PL intensity is normalized in all cases and does not represent any excitation density or detuning-dependent emission intensity changes. Solid lines represent σ^{++} polarization and dashed lines σ^{+-} polarization.

drastically when the system is brought into the nonlinear emission regime, as can be observed in the right panels of figure 12, which correspond to an excitation power density of 60 W cm^{-2}, and the emission stems from the branch with the largest photonic content. For $\delta = +15$ meV the co-polarized emission ($\sigma^+\sigma^+$) is considerably larger than the counter-polarized ($\sigma^+\sigma^-$); the difference becomes even larger and the decay rates also increase at $\delta = +8$ meV. However, the intensities become comparable close to resonance ($\delta = 0$ meV) and the counter-polarized emission becomes dominant for negative detunings.

The time evolution of the circular polarization is depicted in figure 13. The open points correspond to the low excitation regime, which shows a dynamics of the polarization independent of the detuning and very similar to that found for bare excitons in QWs. The traces with the full symbols are taken at an excitation density of 60 W cm^{-2} and demonstrate the very rich behaviour of the polarization when the cavity is in the nonlinear emission regime. At positive detunings, $\mathcal{P}$ is positive and it increases up to its maximum value, which can be as high as 90%, in 20 ps; subsequently $\mathcal{P}$ decreases to zero. The rise of the polarization ($0 < t < 20$ ps) can be interpreted as follows: the initial σ^+-polarized pulse creates a larger $+1$

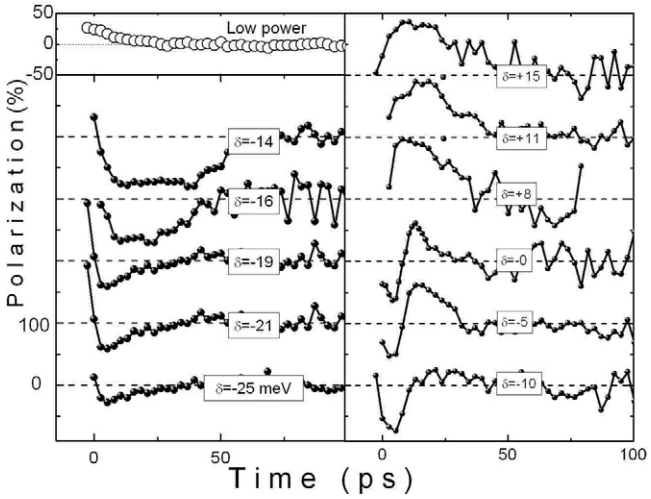

Figure 13. Time evolution of the polarization for sample C1 at different detunings, from $\delta = -25$ to $+15$ meV, for an excitation power density of 60 W cm^{-2} (solid points). A representative evolution at low power, 2 W cm^{-2}, is depicted with open symbols. Each curve is offset by 100%, except the curves for low power and those corresponding to $\delta = -25$ meV and $\delta = -10$ meV.

spin population. A fast scattering process will bring all the photocreated excitons to the cavity mode before any spin relaxation can occur, which will result in a larger $+1$ spin population of $\boldsymbol{K} \sim 0$ states at $t = 0$. This initial $+1$ spin population will act as a seed for the stimulated scattering process and therefore a large number of $+1$ spins will be transferred to $\boldsymbol{K} \sim 0$ states. The radiative recombination of this population will result in a bigger σ^+-polarized emission, i.e. a very large positive polarization. After reaching the maximum $+1/-1$ spin population difference ($t \sim 20$ ps) the $+1$ spin population disappears very quickly through the σ^+-polarized stimulated emission process, taking the polarization to zero ($20 < t < 40$ ps). $\mathcal{P}$ presents a very short time interval of negative values, when δ is close to zero, followed by a maximum, before $\mathcal{P}$ decreases steadily to zero. At negative detunings, $\mathcal{P}$ becomes basically negative, reaching values as large as -75% for $\delta \sim -12$ meV. It even shows a plateau lasting $\sim$30 ps at $\delta = -14$ meV, before the absolute values of $\mathcal{P}$ begin to decrease when the detuning is further increased to negative values. This behaviour is related to the spin-selective polariton–polariton stimulated scattering to the final state, which is strongly dependent of the exciton–cavity detuning.

In the case of $\delta < 0$, the initial σ^+-polarized pulse creates a larger $+1$ spin population, which is reflected at $\boldsymbol{K}_\parallel \sim 0$ by the positive polarization at $t = 0$. The relaxation of the non-resonantly created polaritons to $\boldsymbol{K}_\parallel \sim 0$ is governed by the FSS scattering. Nevertheless, the scattering to the -1 spin states is more efficient than to $+1$ spin states. The accumulation of -1 spin polaritons results in a larger σ^--polarized emission and, therefore, a very large negative polarization. This negative polarization could be attributed to a resonant excitation of light hole excitons; however, this possibility can be discarded by energy arguments (the excitation energy is always at least 30 meV above the light–hole exciton resonance) and furthermore, such a resonant excitation would lead to a negative initial polarization degree, in contrast with the experimental findings.

The different scattering efficiencies might be related to an energy splitting, Δ, observed between the two circularly polarized component of the PL at very short times. This splitting,

which is mirroring the different energies of the $+1$ and the -1 spin levels, increases with excitation power, saturating at $\sim$0.5 meV for 20 W cm^{-2} [50]. In the case of $\delta > 0$, the splitting is observed only for the UP branch. At negative (positive) detunings, the energy of the -1 ($+1$) spin states at $\boldsymbol{K}_{\parallel} \sim 0$ is smaller than that of the $+1$ (-1) spin states; this fact, in addition with the differences in the $+1/-1$ stimulated scattering processes, would account for the large σ^- (σ^+)-polarized emission intensity and the observed negative (positive) polarization. The physical origin of this energy splitting between the two spin states at $\boldsymbol{K}_{\parallel} \sim 0$ still needs to be clarified, but it is likely to account for the reversal of the polarization degree of the PL with changing the exciton–cavity detuning. The splitting would be compatible with a decrease in the light–matter interaction strength for the majority polaritons ($+1$), which are initially created by the σ^+-polarized excitation, as compared to that of the minority (-1) polaritons. This would imply that, for negative (positive) detuning, the $+1$ states would lie above (below) the -1, rendering a $\Delta < 0$ (> 0) as borne out by our results. However, our experiments show that, with increasing excitation density, an initial blue shift of 0.5 meV for both ± 1 states, without any splitting, is followed by a red shift of the -1 polaritons, while the $+1$ remain at the same energy [51]. Therefore, the coupling strength of the $+1$ polaritons does not decrease, invalidating the previous argument. Note that the appearance of the splitting occurs concomitantly with the developing of negative values of the polarization and that both the splitting and $\mathcal{P}$ saturate simultaneously. The fact that the splitting increases with excitation power density indicates that it could originate from exciton–exciton interactions. An existing theory for bare excitons would qualitatively explain the splitting and the ± 1 level ordering, as a result of exchange and vertex corrections to the self-energies [98], but only for $\delta < 0$. Recently a quantum theory of momentum and spin relaxation of polaritons in microcavities, that takes into account self-consistently stimulated scattering and spin-relaxation processes, attributes the observed beats between right- and left-circularly polarized PL to a giant longitudinal–transverse splitting of the polaritons at the bottleneck that mixes their spin states and shows that the effect is strongly sensitive to the bosonic stimulation of polariton scattering [56]. The polarization oscillates with a period proportional to the inverse of the TE–TM splitting and the beats are sensitive to the pumping power due to the interplay between stimulated scattering and spin rotation. However, the theory does not reproduce the fact that the oscillations also take place at $\boldsymbol{K}_{\parallel} = 0$ and $\delta = 0$ (the TE–TM splitting vanishes at this point); one needs to consider a negative detuning ($\delta = -10$ meV) to obtain oscillations at $\boldsymbol{K}_{\parallel} = 0$. In the latter case, where a strong bottleneck effect arises (i.e. the maximum of polariton population corresponds to a nonzero in-plane wave vector of light), the polarization of all lower states is found to be strongly influenced by the bottleneck effect. These experiments and the theoretical frame explaining them demonstrate that the conservation of the spin coherence is compatible with fast relaxation processes.

Finally, let us mention that a detailed study of the spin-dependent polariton dynamics for CdTe microcavities as a function of detuning can be found in the work of Aichmayr *et al* [51].

7. Coexistence of strong and weak coupling

Increasing the pump power in a microcavity raises the carrier density, then screening and phase–space filling effects decrease the exciton oscillator strength resulting in a decrease of the Rabi splitting [85]. As a consequence, when the excitation power increases, a transition from the strong- to the weak-coupling regime occurs and the emission of the system shifts from the polariton energy to the bare-cavity mode energy [99]. The integrated emission intensity, for σ^+ excitation, of the two orthogonal polarizations (σ^+, solid dots; σ^-, open dots) is plotted in figure 14 for sample C2, at a negative detuning of -14 meV, as a function of excitation

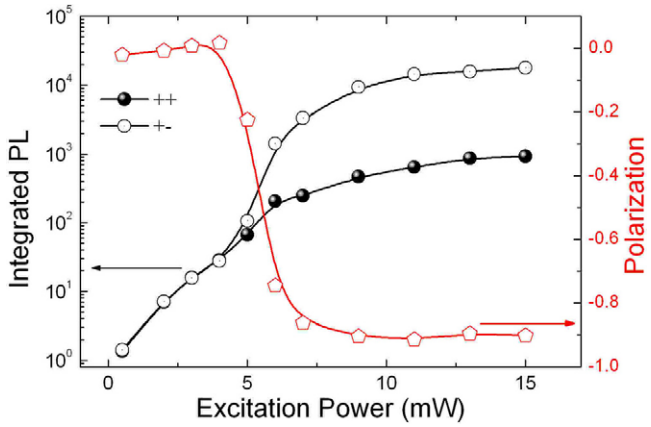

Figure 14. Time-integrated LPB emission intensities for the co-polarized (solid dots) and counter-polarized (open dots) components as a function of excitation power for sample C1 at $\delta = -13.2$ meV. The pentagons represent the corresponding values of the polarization.

power together with the degree of polarization (pentagons). As the excitation power is initially increased a superlinear increase of the emission is observed for both polarizations. A further increase of the power above ∼5 mW (first threshold) originates a dramatic increase of the σ^- emission, while the signal with σ^+ polarization presents a much less marked dependence with power. This effect is the one responsible for the appearance of negative degrees of polarization such as the ones depicted in figure 13. A second threshold is obtained at a power of ∼10 mW, when the intensities of the σ^- emission practically saturate and the σ^+ PL only increases slightly with power. This behaviour of the polarized emission results in the appearance of a negative degree of polarization at the first threshold, which reaches values as big as −90%. The excitation density-dependent energy shifts of the emission have to be observed carefully, in order to establish whether the system is in the strong- or the weak-coupling regime. This analysis shows [51] that, on increasing the excitation density, both emission peaks shift to higher energies, obtaining a blue shift of ∼0.5 meV at 5 mW. This value is smaller than the separation between bare and coupled modes at this detuning, confirming the endurance of the strong coupling. This dependence changes for higher densities: the σ^{++} emission energy remains approximately constant, whereas the σ^{+-} peak red shifts when the power is further increased, which leads to an energy splitting between the two spin components [51]. This happens at the same density where the negative polarization sets in. Therefore, for the CdTe system one can conclude that even under non-resonant excitation the polaritons remain in the strong coupling regime for the powers reported in figure 14.

The situation is, however, quite different when considering the InGaAs system, where a transition from the strong- to the weak-coupling regime is observed at relatively low powers under conditions of non-resonant excitation. Figure 15(a) shows the integrated emission intensity for the two orthogonal polarizations (σ^+, solid dots; σ^-, open dots), for sample A at resonance ($\delta = 0$), as a function of excitation power for σ^+ excitation. Again a similar behaviour to that reported in figure 14 can be observed, but at different excitation powers and with different sign of the polarization degree. An initially slow increase of the emission is observed for both polarizations. A further increase of the power above ∼0.8 mW (first threshold) produces a dramatic increase of the σ^+ emission, while the signal with σ^- polarization presents a much less marked dependence with power. A second threshold is obtained at a power of ∼1.2 mW, when the intensities of both emissions practically saturate.

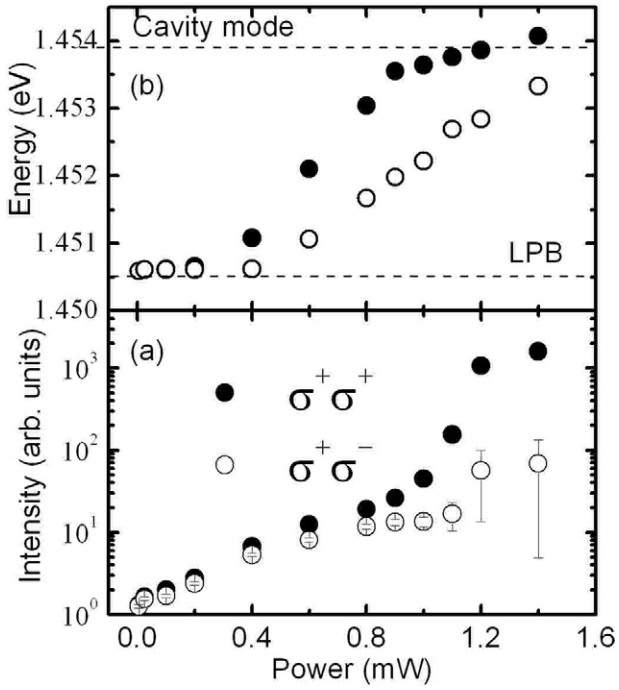

Figure 15. (a) Time-integrated LPB emission intensities for the co-polarized (solid dots) and counter-polarized (open dots) components as a function of excitation power for sample A at $\delta = 0$ meV. (b) LPB energies at the maximum of their time evolution as a function of the excitation power for the two polarizations of the emission σ^+ (●) and σ^- (○).

However, an analysis of the excitation density-dependent energy shifts reveals that in this case the system undergoes a spin-dependent transition from the strong- to the weak-coupling regime when the power is increased. This behaviour can be observed in figure 15(b), where the energies of the emission are plotted versus excitation power: at very low powers the emission energy is the same for σ^+ and σ^- polaritons, corresponding to that of the LPB; however, a splitting appears at an excitation power of 0.4 mW. Both polarizations undergo a gradual loss of strong coupling with increasing intensity, but the resulting Rabi splitting is different for σ^+ and σ^- polaritons under the same excitation conditions, as has been also observed in the literature [19, 100]. At 1 mW the σ^+ polaritons are in the weak-coupling regime (as can be readily inferred by its position that has reached the bare-cavity energy), while the σ^- polaritons energy is still well below the cavity mode energy and a complete loss of the strong coupling is reached only at 1.7 mW. The origin of this breaking of the spin degeneracy at high exciton density can be discussed on the light of the changes in the exciton oscillator strength. Two processes are likely responsible of these changes in a QW: the phase–space filling, a blocking mechanism due to the exclusion principle, and the modification of the e–h interaction induced by the presence of other e–h pairs [83]. Both exchange (also a consequence of the exclusion principle) and long-range Coulomb effects can modify the e–h interaction. In a 2D system, the effect of the long-range Coulomb effect can be disregarded [83].

To have a deeper understanding of the dependence of the energy splitting on the relative populations of opposite spin, it is useful to examine the occupation factors of the σ^+ and σ^- polaritons as a function of excitation power. This analysis yields that the occupation factor

$n_f^{\sigma+}$ reaches unity at 1.1 mW, when the emission is fully photonic, and a laser-like emission (100% σ^+-polarized) is observed [101]. Plotting the σ^+ and σ^- LPB peak energies versus the respective occupation factors, in the region below where the strong coupling is completely lost, the two curves are exactly superimposed. Therefore one can conclude that the energies of emission of the polarized polaritons, and consequently the regime of existence of polaritons (strong versus weak coupling), is fully determined by the occupation factor of the polaritons with a given spin and does not depend strongly on the total population of both kinds of polaritons [101]. This strong dependence of the emission energies on the relative populations of opposite spin has been explained for an exciton gas in a QW through an exciton–exciton interaction model [98]. According to this model the energy level splitting is due to many-body inter-excitonic exchange, while intra-excitonic exchange is responsible for the spin relaxation time. The energy difference of the spin levels is directly proportional to the polarization [98], a fact that we and others [100] have also found in microcavities. However, in QWs the σ^+ energy remains almost constant with increasing excitation intensity; the splitting is mainly due to a red shift of the σ^- emission energy and it vanishes, together with the degree of polarization, in a time of the order of 50 ps. In spite of a good qualitative agreement of the amount of the energy splitting on the relative difference of the unbalanced populations, further investigations are needed to obtain a better understanding of this mechanism in a semiconductor microcavity. In fact, the dynamics of the emission is strongly modified by the cavity and the decreasing Rabi splitting effect on the polaritons energy has to be added in the calculations of the absolute position of the PL peaks.

8. Pinning of the linear polarization

In the quest for polariton lasing, one of the very important issues is the polarization dynamics in microcavities. A spontaneous build-up of the linear polarization in the emission of polariton lasers has been predicted theoretically [68]. According to this theory, the direction of linear polarization would be spontaneously chosen by the system, and it would vary randomly from one experiment to another. Only recently has the degree of linear polarization of the emission been studied in microcavities of InGaAs [62], also paying special attention to its angular dependence [60], and of CdTe [59]. The work of Krizhanovskii *et al* [62] suggests that some built-in anisotropy may affect the polarization relaxation of polaritons. Our studies both in sample A and C2 demonstrate experimentally that the linear polarization of emission of polariton lasers can be pinned to one of crystallographic axes. This pinning comes from the optical anisotropy of microcavities, which may be caused by a small birefringence in the mirrors and cavity, by the exciton localization at QW interfaces or by the QW intrinsic anisotropy. A careful analysis has led us to conclude that the first option is the most likely one [63].

Figures 16(a), (b) display the time evolution of the two linearly polarized components of the PL (semi-logarithmic scale) from the LPB of sample C2 after horizontally polarized excitation for excitation densities below (6 W cm^{-2}, spontaneous) and above (56 W cm^{-2}, stimulated) the stimulated scattering threshold, respectively. The decay time amounts to 130 ps/15 ps in the spontaneous/stimulated regime. It can be clearly seen in both figures that the intensity of the vertically polarized emission (dashed line) is larger than that of the horizontally polarized one (solid line) and that this difference of the intensities is visible all through the duration of the emission. This becomes more evident looking at the time evolution of the degree of linear polarization of the emission (obtained from the time evolution traces), $\mathcal{P}$, which is displayed in figures 16(c), (d), for the same conditions as in figures 16(a), (b). In the spontaneous regime (figure 16(c)), a build-up of a negative polarization is observed during the

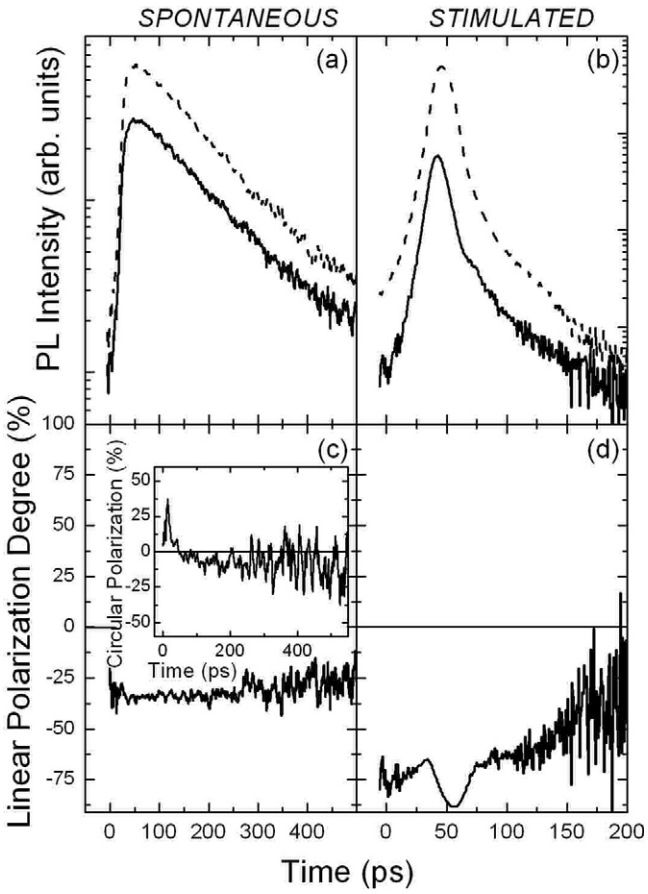

Figure 16. (a), (b) Time evolution of the PL, in semi-logarithmic scale, measured under non-resonant excitation with horizontally polarized light of the LPB for sample C2 in the spontaneous (6 W cm^{-2}) and stimulated (56 W cm^{-2}) regimes, respectively. Solid/dashed lines are linearly horizontally and vertically polarized signals. (c), (d) Temporal profiles of the linear polarization degree in the spontaneous and stimulated regimes, respectively. The inset shows the decay of the circular polarization degree under circular-polarized pumping in the spontaneous regime.

first 50 ps, after which a net polarization of ∼35% is recorded as long as there is any measurable signal. In a similar way, a polarization degree of −65% is obtained for a larger excitation density (figure 16(d)) once in the stimulated regime, in which the linear polarization degree reaches its maximum value (∼90%). This remarkable enhancement of the linear polarization degree is due to the bosonic stimulation effect, triggered by the large occupation numbers of the ground state obtained in the stimulated scattering regime.

In both regimes, the decay time of the linear polarization degree is of the order of 1 ns, i.e. much longer than the intensity decay time. The inset shows the time evolution of the circular polarization degree of the PL obtained under similar conditions as in the experiment described above but using circularly polarized excitation/detection: it shows a fast decay on a timescale of 40 ps and then becomes negligible. Thus, surprisingly, the linear polarization decay time is much longer than all the other characteristic times of the system. Furthermore, the fact that $\mathcal{P}$ is negative implies a 90° rotation of the polarization plane of the emission with respect to that of the excitation. A rotation of the excitation plane by 90° (exciting the PL with vertically

polarized light) still results in the vertically polarized component of the PL being stronger all through the duration of the emission. These experimental results show that the polarization of the emission is pinned to one of the crystallographic axes of the structure. This pinning has been confirmed by supplementary experiments performed with the sample rotated 90°, returning to same spot and using similar excitation conditions. In this case, we have also found that the preferential orientation for the polarization of the emission is rotated by 90°, thus confirming the pinning along the same crystal axis as before.

We interpret these striking effects, i.e. the long decay time of $\mathcal{P}$ and the pinning of the linear polarization, as a consequence of a splitting of the polariton ground state. This splitting can arise from either a splitting of the exciton resonance into a linearly polarized radiative doublet or from a splitting of the photon eigenmodes of the cavity polarized vertically and horizontally, which can be caused by the fluctuations in the photonic potential arising from misfit dislocations in the Bragg mirrors [64, 102]. It is worth mentioning that the longitudinal–transverse splitting of exciton–polaritons, which is responsible for polariton spin relaxation in the excited states, is always zero at $k = 0$ [56].

The inset in figure 17(a) shows the PL of sample C2 under cw excitation (3 mW) at 1.705 eV with horizontally polarized light on a spot of diameter 2.5 μm at a detuning of -15 meV. The peak positions of the emission polarized horizontally (solid dots) and vertically (open dots) are plotted in figure 17(a) versus lattice temperature. The resulting splittings from the difference of the peak positions of both polarized emission are compiled in figure 17(b), and the linear polarization degree is shown in figure 17(c) as a function of T. These cw experiments confirm the existence of an energy splitting between the two linearly polarized components of the PL (figure 17(b)) and show that the component lying at higher energies always has a larger intensity than that of the counter-polarized one, indicating a non-thermal origin of the polarization. These experiments also show that the splitting is very robust. The linear polarization and the splitting have a similar temperature dependence, monotonically decreasing with T and both vanishing at $T \sim 100$ K, thus confirming the direct relationship between the energy splitting and the observed linear polarization degree.

The origin of the splitting has been profusely discussed in [63], and it has been shown that a slight birefringence of the cavity or the mirrors, which splits the bare photon modes of the microcavity in horizontal and vertical polarizations, is the most probable candidate for this effect. The frequency ω_c of the uncoupled cavity mode is inversely proportional to the refractive index of the cavity material n_c. In an ideal λ-microcavity $\omega_c = 2\pi c/n_c L_c \omega_c$, where L_c is the cavity width. Thus, a small change of n_c leads to a variation of the cavity frequency given by

$$\Delta\omega_c \approx -\frac{\Delta n_c}{n_c}\omega_c. \tag{3}$$

To obtain an energy splitting of 400 μeV, the refractive index of the cavity should vary by about 0.04% between horizontal and vertical polarizations. Such a small variation can be a result of a weak uniaxial strain in the plane of the cavity.

9. Conclusions

We have shown that semiconductor microcavities provide an exceptional scenario to study strong radiation–matter interactions in solid-state physics. We have reviewed the temporal dynamics of polaritons in II–VI and III–V based microcavities under non-resonant excitation conditions. We have presented evidence of final-state stimulated scattering and have discussed the spin-dependent emission, which exhibits a remarkably rich behaviour. We have shown

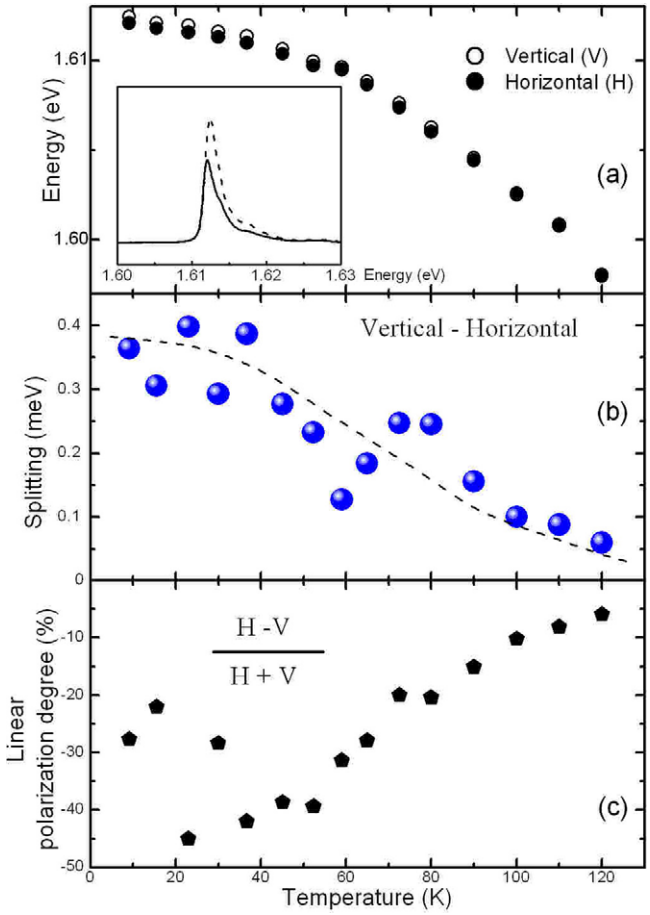

Figure 17. (a) Energies of the LPB for sample C2 under cw excitation with horizontally polarized light as a function of lattice temperature. The inset shows the spectra at 5 K for vertical (dashed lines) and horizontal (solid lines) detection. (b) Splitting between the two orthogonal components of the emission as a function of temperature. (c) Linear polarization degree as a function of temperature.

that the loss of strong coupling for a polariton population of a given spin is determined by the occupation factor of that population and is not strongly influenced by the presence of opposite-spin polaritons. Finally, we have demonstrated a pinning of the linear polarization degree in non-resonantly pumped microcavities, caused by a splitting of the polariton ground state, which is due to a slight birefringence of the cavity or the mirrors.

Acknowledgments

The work was partially supported by the Spanish MEC (MAT2005-01388, NAN2004-09109-C04-04 and Consolider-Ingenio CSD2006-00019), the CAM (S-0505/ESP-0200) and the 'Marie-Curie' MRTN-CT-2003-503677. We are very grateful to E E Mendez, R André and M Skolnick, who kindly supplied the samples used in our studies to the SEMICUAM group in Madrid.

References

[1] Weisbuch C, Nishioka M, Ishikawa A and Arakawa Y 1992 *Phys. Rev. Lett.* **69** 3314
[2] Sermage B, Long S, Abram I, Marzin J Y, Bloch J, Planel R and Thierry-Mieg V 1996 *Phys. Rev.* B **53** 16516
[3] Baumberg J J and Viña L (ed) 2003 *Semicond. Sci. Technol.* **18** (Special Issue on Microcavities)
[4] Keldysh L V and Kozlov A N 1968 *Sov. Phys.—JETP* **27** 521
[5] Hanamura E and Haug H 1977 *Phys. Rep.* **33** 209
[6] Comte C and Noziers P 1982 *J. Physique* **43** 1069
[7] Kira M, Jahnke F, Koch S W, Berger J D, Wick D V, Nelson T R, Khitrova G and and Gibbs H M 1997 *Phys. Rev. Lett.* **79** 5170
[8] Imamoglu A, Ram R J, Pau S and Yamamoto Y 1996 *Phys. Rev.* A **53** 4250
[9] Pau S, Cao H, Jacobson J, Björk G, Yamamoto Y and Imamoglu A 1996 *Phys. Rev.* A **54** R1789
[10] Dang L S, Heger D, Andre R, Boeuf F and Romestain R 1998 *Phys. Rev. Lett.* **81** 3920
[11] Savvidis P G, Baumberg J J, Stevenson R M, Skolnick M S, Whittaker D M and Roberts J S 2000 *Phys. Rev. Lett.* **84** 1547
[12] Huang R, Tassone F and Yamamoto Y 2000 *Phys. Rev.* B **61** R7854
[13] Savvidis P G, Baumberg J J, Stevenson R M, Skolnick M S, Whittaker D M and Roberts J S 2000 *Phys. Rev.* B **62** R13278
[14] Ciuti C, Schwendimann P, Devaud B and Quattropani A 2000 *Phys. Rev.* B **62** R4825
[15] Ciuti C, Schwendimann P and Quattropani A 2001 *Phys. Rev.* B **63** 041303
[16] Baars T, Bayer M, Forchel A, Schäfer F and Reithmaier J P 2000 *Phys. Rev.* B **61** R2409
[17] Stevenson R M, Astratov V N, Skolnick M S, Whittaker D M, Emam-Ismail M, Tartakovskii A I, Savvidis P G, Baumberg J J and Roberts J S 2000 *Phys. Rev. Lett.* **85** 3680
[18] Senellart P, Bloch J, Sermage B and Marzin J Y 2000 *Phys. Rev.* B **62** R16263
[19] Tartakovskii A I, Kulakovskii V D, Krizhanovskii D N, Skolnick M S, Astratov V N, Armitage A and Roberts J S 1999 *Phys. Rev.* B **60** 11293
[20] Senellart P and Bloch J 1999 *Phys. Rev. Lett.* **82** 1233
[21] Boeuf F, André R, Romestain R and Dang L S 2000 *Phys. Rev.* B **62** 2279
[22] Saba M, Ciuti C, Bloch J, Thierry-Mieg V, Andre R, Dang L S, Kundermann S, Mura A, Bongiovanni G, Staehli J L and Deveaud B 2001 *Nature* **414** 731
[23] Richard M, Kasprzak J, André R, Romestain R, Dang L S, Malpuech G and Kavokin A 2005 *Phys. Rev.* B **72** 201301
[24] Deng H, Weihs G, Santori C, Bloch J and Yamamoto Y 2002 *Science* **298** 199
[25] Deng H, Weihs G, Snoke D, Bloch J and Yamamoto Y 2003 *Proc. Natl Acad. Sci.* **100** 15318
[26] Alexandrou A, Bianchi G, Péronne E, Hallé B, Boeuf F, André R, Romestain R and Dang L S 2001 *Phys. Rev.* B **64** 233318
[27] Senellart P, Bloch J, Sermage B and Marzin J Y 2000 *Phys. Rev.* B **62** R16263
[28] Bloch J, Sermage B, Perrin M, Senellart P, André R and Dang L S 2005 *Phys. Rev.* B **71** 155311
[29] Kasprzak J, Richard M, Kundermann S, Baas A, Jeambrun P, Keeling J, Marchetti F M, Szymanska M, André R, Staehli J L, Savona V, Littlewood P, Deveaud B and Dang L 2006 *Nature* **443** 409
[30] Doan T D, Cao H T, Thoai D B T and Haug H 2005 *Phys. Rev.* B **72** 85301
[31] Haug H 2005 *Solid State Commun.* **134** 3
[32] Doan T D, Cao H T, Thoai D B T and Haug H 2006 *Phys. Rev.* B **74** 115316
[33] Eastham P R and Littlewood P B 2000 *Solid State Commun.* **116** 357
[34] Eastham P R and Littlewood P B 2001 *Phys. Rev.* B **64** 235101
[35] Szymanska M H and Littlewood P B 2002 *Solid State Commun.* **124** 103
[36] Szymanska M H, Littlewood P B and Simons B D 2003 *Phys. Rev.* A **68** 013818
[37] Keeling J, Eastham P R, Szymanska M H and Littlewood P B 2005 *Phys. Rev.* B **72** 115320
[38] Keeling J, Eastham P R, Szymanska M H and Littlewood P B 2004 *Phys. Rev. Lett.* **93** 226403
[39] Littlewood P B, Eastham P R, Keeling J M J, Marchetti F M, Simons B D and Szymanska M H 2004 *J. Phys.: Condens. Matter* **16** S3597
[40] Keeling J, Levitov L S and Littlewood P B 2004 *Phys. Rev. Lett.* **92** 176402
[41] Marchetti F M, Simons B D and Littlewood P B 2004 *Phys. Rev.* B **70** 155327
[42] Marchetti F M, Szymanska M H, Eastham P R, Simons B D and Littlewood P B 2004 *Solid State Commun.* **134** 111
[43] Keeling J 2006 *Phys. Rev.* B **74** 155325
[44] Szymanska M H, Keeling J and Littlewood P B 2006 *Phys. Rev. Lett.* **96** 230602
[45] Marchetti F M, Keeling J, Szymanska M H and Littlewood P B 2006 *Phys. Rev. Lett.* **96** 066405

[46] Lagoudakis P G, Savvidis P G, Baumberg J J, Whittaker D M, Eastham P R, Skolnick M S and Roberts J S 2002 *Phys. Rev.* B **65** R161310
[47] Renucci P, Amand T and Marie X 2003 *Semicond. Sci. Technol.* **18** S361
[48] Martín M D, Viña L, Son J K and Mendez E E 2001 *Solid State Commun.* **117** 267
[49] Martín M D, Viña L and Méndez E E 2001 *Solid State Commun.* **119** 259
[50] Martin M D, Aichmayr G, Viña L and André R 2002 *Phys. Rev. Lett.* **89** 077402
[51] Aichmayr G, Martín M D and André R 2003 *Semicond. Sci. Technol.* **18** S368
[52] Martín M D, Aichmayr G, Viña L and André R 2004 *Semicond. Sci. Technol.* **19** S365
[53] Kłopotowski Ł, Amo A, Martín M D, Viña L and André R 2005 *Phys. Status Solidi* a **202** 357
[54] Kavokin A, Lagoudakis P G, Malpuech G and Baumberg J J 2003 *Phys. Rev.* B **67** 195321
[55] Kavokin A V, Shelykh I A, Kavokin K V, Bigenwald P and Malpuech G 2003 *Phys. Status Solidi* c **0** 1405
[56] Kavokin K V, Shelykh I A, Kavokin A V, Malpuech G and Bigenwald P 2004 *Phys. Rev. Lett.* **92** 017401
[57] Shelykh I, Malpuech G, Kavokin K V, Kavokin A V and Bigenwald P 2004 *Phys. Rev.* B **70** 115301
[58] Shelykh I, Kavokin K V, Kavokin A V, Malpuech G, Bigenwald P, Deng H, Weihs G and Yamamoto Y 2004 *Phys. Rev.* B **70** 035320
[59] Martín M D, Ballarini D, Amo A, Kłopotowski Ł, Viña L, Kavokin A V and André R 2005 *Phys. Status Solidi* c **2** 3880
[60] Amo A, Martín M D, Ballarini D, Viña L, Sanvitto D, Skolnick M S and Roberts J S 2005 *Phys. Status Solidi* c **2** 3868
[61] Kavokin K V, Renucci P, Amand T, Marie X, Senellart P, Bloch J and Sermage B 2005 *Phys. Status Solidi* c **2** 763
[62] Krizhanovskii D N, Sanvitto D, Shelykh I A, Glazov M M, Malpuech G, Solnyshkov D D, Kavokin A, Ceccarelli S, Skolnick M S and Roberts J S 2006 *Phys. Rev.* B **73** 073303
[63] Kłopotowski Ł, Martín M D, Amo A, Viña L, Shelykh I A, Glazov M M, Kavokin G M A and André R 2006 *Solid State Commun.* **139** 511
[64] Gurioli M, Bogani F, Cavigli L, Gibbs H, Khitrova G and Wiersma D S 2005 *Phys. Rev. Lett.* **94** 183901
[65] Renucci P, Amand T, Marie X, Senellart P, Bloch J, Sermage B and Kavokin K V 2005 *Phys. Rev.* B **72** 075317
[66] Malpuech G, Glazov M M, Shelykh I A, Bigenwald P and Kavokin K V 2006 *Appl. Phys. Lett.* **88** 111118
[67] Shelykh I A, Rubo Y G, Malpuech G, Solnyshkov D D and Kavokin A 2006 *Phys. Rev. Lett.* **97** 066402
[68] Laussy F P, Shelykh I A, Malpuech G and Kavokin A 2006 *Phys. Rev.* B **73** 035315
[69] Khitrova G, Gibbs H M, Jahnke F, Kira M and Koch S W 1999 *Rev. Mod. Phys.* **71** 1591
[70] Savona V, Permarocchi C, Quattropani A, Schwendimann P and Tassone F 1999 *Phase Transit.* **68** 169
[71] Kavokin A and Malpuech G (ed) 2003 *Cavity Polaritons* vol 31 (Amsterdam: Elsevier)
[72] Deveaud B (ed) 2005 *Phys. Status Solidi* b **242** (Physics of Semiconductor Microactivities)
[73] Savvidis P G, Baumberg J J, Porras D, Whittaker D M, Skolnick S and Roberts J S 2002 *Phys. Rev.* B **65** 73309
[74] Andreani L C 1994 *Phys. Lett.* A **192** 99
[75] Aichmayr G 2001 *Thesis: Dynamics of Light–Matter Interaction in Semiconductor Nanostructures* Universidad Autónoma, Madrid (Spain)
[76] Madelung O, Schulz M and Weiss H (ed) 1982 *Landolt-Börnstein* vol 17 (Berlin: Springer)
[77] Shah J (ed) 1996 *Ultrafast Spectroscopy of Semiconductors and Semiconductor Heterostructures* (Berlin: Springer)
[78] Abram I, Sermage B, Long S, Bloch J, Planel R and Thierry-Mieg V 1996 *Microcavities and Photonic Bandgaps: Physics and Applications* (*NATO ASI Series E 324*) ed J Rarity and C Weisbuch (Dordrecht: Kluwer Academic)
[79] Damen T C, Viña L, Cunningham J E, Shah J and Sham L J 1991 *Phys. Rev. Lett.* **67** 3432
[80] Muñoz L, Pérez E, Viña L and Ploog K 1995 *Phys. Rev.* B **51** 4247
[81] Tassone F, Piermarocchi C, Savona V, Quattropani A and Schwendimann P 1997 *Phys. Rev.* B **56** 7554
[82] Peyghambarian N, Gibbs H M, Jewell J L, Antonetti A, Migus A, Hulin D and Mysyrowicz A 1984 *Phys. Rev. Lett.* **53** 2433
[83] Schmitt-Rink S, Chemla D S and Miller D A B 1985 *Phys. Rev.* B **32** 6601
[84] Hulin D, Mysyrowicz A, Antonetti A, Migus A, Masselink W T, Morkoc H, Gibbs H M and Peyghambarian N 1986 *Phys. Rev.* B **33** 4389
[85] Houdré R, Gibernon J L, Pellandini P, Stanley R P, Osterle U, Weisbuch C, O'Gorman J, Roycroft B and Ilegems M 1995 *Phys. Rev.* B **52** 7810
[86] Porras D and Tejedor C 2003 *Phys. Rev.* B **67** R161310
[87] Houdré R, Weisbuch C, Stanley R P, Oesterle U and Ilegems M 2000 *Phys. Rev. Lett.* **85** 2793
[88] Erland J, Mizeikis V, Langbein W, Jensen J R and Hvam J M 2001 *Phys. Rev. Lett.* **86** 5791
[89] Greiner M, Mandel O, Hänsch T W and Bloch I 2002 *Nature* **419** 51

[90] Dasbach G, Dremin A A, Bayer M, Kulakovskii V D, Gippius N A and Forchel A 2002 *Phys. Rev.* B **65** 245316
[91] Renucci P, Amand T and Marie X 2003 *Physica* E **17** 329
[92] Shelykh I A, Viña L, Kavokin A V, Galkin N G, Malpuech G and André R 2005 *Solid State Commun.* **135** 1 at press doi:10.1016/j.spmi.2007.03.029
[93] Martín M D, Ballarini D, Amo A, Viña L and André R 2007 *Superlatt. Microstruct.* at press
[94] D'yakonov M I and Perel' V I 1984 Theory of optical spin orientation of electrons and nuclei in semiconductors *Optical Orientation* ed F Maier and B P Zakharchenya (Amsterdam: Elsevier) p 11
[95] Pikus G E and Titkov A N 1984 Spin relaxation under optical orientation in semiconductors *Optical Orientation* ed F Maier and B P Zakharchenya (Amsterdam: Elsevier) p 73
[96] Langbein W, Zimmermann R, Runge E and Hvam J M 2000 *Phys. Status Solidi* b **221** 349
[97] Zimmermann R, Langbein W, Runge E and Hvam J M 2001 *Physica* E **10** 40
[98] Fernández-Rossier J, Tejedor C, Muñoz L and Viña L 1996 *Phys. Rev.* B **54** 11582
[99] Butté R, Delalleau G, Tartakovskii A I, Skolnick M S, Astratov V N, Baumberg J J, Malpuech G, Carlo A D, Kavokin A V and Roberts J R 2002 *Phys. Rev.* B **65** 205310
[100] Quochi F, Staehli J, Oesterle U, Deveaud B, Bongiovanni G, Mura A and Saba M 1999 *24th Int. Conf. Phys. Semiconduct.* ed D Gershoni (Singapore: World Scientific) CDROM 0565.pdf, IV-G-2
[101] Ballarini D, Amo A, Martin M D, Viña L, Sanvitto D, Skolnick M S and Roberts J S 2007 *Superlatt. Microstruct.* at press doi:10.1016/j.spmi.2007.03.023
[102] Langbein W 2006 private communication